The Astronomical Journal, 159:292 (15pp), 2020 June https://doi.org/10.3847/1538-3881/ab8f90

Further Investigation on Chromospheric and Prominence Activity of the RS Canum Venaticorum Star SZ Piscium

Dongtao Cao[1,2], Shenghong Gu[1,2,3], U. Wolter[4], M. Mittag[4], and J. H. M. M. Schmitt[4]
[1] Yunnan Observatories, Chinese Academy of Sciences, Kunming 650216, People's Republic of China; dtcao@ynao.ac.cn, shenghonggu@ynao.ac.cn
[2] Key Laboratory for the Structure and Evolution of Celestial Objects, Chinese Academy of Sciences, Kunming 650216, People's Republic of China
[3] School of Astronomy and Space Science, University of Chinese Academy of Sciences, Beijing 101408, People's Republic of China
[4] Hamburger sternwarte, Hamburg D-21029, Germany
Received 2020 February 19; revised 2020 April 16; accepted 2020 April 30; published 2020 June 3

Abstract

To continue our study on chromospheric activity and detection for possible prominence events of the very active RS Canum Venaticorum star SZ Piscium (SZ Psc), long-term high-resolution spectroscopic observations were obtained during several observing runs from 2014 to 2018. Based on the spectral subtraction technique, the chromospheric emission of the Ca II IRT (λ8662, λ8542, and λ8498), H_α, Na I D_1, D_2 doublet, H_β, and Ca II H & K lines is mainly associated with the K1 IV primary star of the SZ Psc system, in good agreement with the previous studies, and the F8 V secondary star also shows some chromospheric emission, implying its active chromosphere. Moreover, an optical flare characterized by the He I D_3 line emission together with stronger emission in the other indicators was detected. Furthermore, two chromospheric active longitudes around the two quadratures of the system were identified for most of the time, and the chromospheric activity shows significant changes during a few orbital cycles. The chromospheric activity level seems to show a long-term variation during our observations. There were some excess absorption features in the subtracted H_α line and the other activity indicators, which would be caused by prominence-like materials associated with the K1 IV primary star of the system. Prominence materials could absorb the chromospheric emission and continuum from the K1 IV primary star and even the F8 V secondary one.

Unified Astronomy Thesaurus concepts: Stellar activity (1580); Close binary stars (254); High resolution spectroscopy (2096); Stellar chromospheres (230); Stellar flares (1603)

Supporting material: machine-readable tables

1. Introduction

Solar-type activity phenomena including starspots, plages, flares, and prominences, arose from a powerful magnetic dynamo generated by the interplay between the turbulent motions in the convection zone and the stellar differential rotation have been widely observed in cool stars (Schrijver & Zwaan 2000). Among these activity phenomena, stellar prominences have been reported for the first time by Robinson & Collier Cameron (1986) as transient absorption features passing through the rotationally broadened H_α profile of the rapidly rotating K0 dwarf star AB Dor. Such absorption transients are thought to be caused by prominence materials magnetically supported high above the stellar photosphere and forced to corotate with the star, which can scatter the underlying chromospheric emission out of the line of sight as they transit the stellar disk (Collier Cameron & Robinson 1989a, 1989b). Up to now, similar prominence features have been detected on several rapidly rotating single active stars, such as AB Dor (Collier Cameron & Robinson 1989a, 1989b), G-type dwarfs in the α Per cluster (Collier Cameron & Woods 1992), BO Mic (Jeffries 1993; Dunstone et al. 2006; Wolter et al. 2008), HK Aqr (Byrne et al. 1996), PZ Tel (Barnes et al. 2000), RX J1508.6−4423 (Donati et al. 2000) and RE 1816+514 (Eibe 1998), and on a number of RS Canum Venaticorum (RS CVn)-type binary systems (Hall & Ramsey 1992), especially on the SZ Piscium (SZ Psc) system (Zhang & Gu 2008; Cao & Gu 2012; Cao et al. 2019). At Yunnan observatories, we began a long-term high-resolution spectroscopic monitoring project to search for prominence-like materials and study the active chromosphere on a number of RS CVn-type systems (Cao & Gu 2012, 2015, 2017; Cao et al. 2019).

The star SZ Psc (SAO 128041, HD 219113) is a triple-lined spectroscopic system, which consists of an eclipsing binary with a K1 IV primary and a F8 V secondary in a circular orbit with a period of about 3.97 days (Jakate et al. 1976), and a tertiary component (Eaton & Henry 2007; Glazunova et al. 2008; Xiang et al. 2016). The binary of the SZ Psc system belongs to the RS CVn class of variable stars having strong magnetic activity, such as starspots (Eaton & Hall 1979; Lanza et al. 2001; Kang et al. 2003; Eaton & Henry 2007; Xiang et al. 2016) and intense chromospheric emission in the Mg II h & k, Ca II H & K, H_α, and Ca II IRT lines (Jakate et al. 1976; Bopp 1981; Ramsey & Nations 1981; Huenemoerder & Ramsey 1984; Fernández-Figueroa et al. 1986; Popper 1988; Frasca & Catalano 1994; Kang et al. 2003; Eaton & Henry 2007; Zhang & Gu 2008; Cao & Gu 2012), and more often shows very unusual behavior in the H_α line profile probably caused by particularly stellar magnetic activity events (Bopp 1981; Ramsey & Nations 1981; Huenemoerder & Ramsey 1984; Zhang & Gu 2008; Cao & Gu 2012).

Therefore, the SZ Psc system is a notable target star to study its magnetic activity, and more recently a series of probably associated magnetic activity phenomena, including possibly flare-related prominence activation, a strong optical flare event, and post-flare loops were reported in our previous paper (for a detailed description see Cao et al. 2019, hereafter C19). To further investigate the chromospheric activity and possibly prominence activity events in the SZ Psc system in detail, we

present more new high-resolution spectroscopic observations sometimes with much higher temporal cadence.

The details of new spectroscopic observations and data reduction are described in Section 2, and in Section 3, the spectral analysis procedure, the behavior of chromospheric activity indicators, an optical flare, and the chromospheric activity variation are given and investigated. In Section 4, some unusual excess absorption features presented in the subtraction of chromospheric activity indicators are discussed. Finally, we give a summary on our study in Section 5.

2. Spectroscopic Observations and Their Reduction

High-resolution spectroscopic observations of the SZ Psc system were performed during several observing runs from 2014 to 2018. Most of the spectroscopic observations were carried out with the 2.16 m telescope at the Xinglong station of National Astronomical Observatories and the 2.4 m telescope (Fan et al. 2015) at the Lijiang station of Yunnan observatories, Chinese Academy of Sciences, respectively. The same fiber-fed High-Resolution Echelle Spectrograph (HiRES), which has a resolving power of $R = \lambda/\Delta\lambda \simeq 48{,}000$ over the wavelength range from 3900 to 9500 Å, was equipped to both telescopes and the 4096×4096 pixel CCD detectors were respectively used to record the echelle spectra during our observations.

Moreover, there are some spectroscopic observations were made using the TIGRE 1.2 m telescope of Hamburg Observatory, Germany (Schmitt et al. 2014). TIGRE is a robotic telescope located at the La Luz Observatory in Central Mexico near Guanajuato and equipped with the fiber-fed Heidelberg Extended Range Optical Spectrograph. TIGRE spectra have a resolving power of $R = \lambda/\Delta\lambda \simeq 20{,}000$, covering a wavelength range of 3800–5700 and 5800–8800 Å in the blue and red region, respectively.

We give an observing log of SZ Psc in Table 1, which includes the telescope we used, the observing date, the heliocentric Julian date (HJD), the orbital phase, and the exposure time. The orbital phases are determined using the ephemeris

$$\mathrm{HJD} = 2{,}449{,}284.4483 + 3\overset{\mathrm{d}}{.}96566356 \times E \qquad (1)$$

from Eaton & Henry (2007), where the epoch corresponds to the conjunction with the K1 IV primary component of the SZ Psc system in front.

Some slowly rotating inactive stars, HR 7690 (K1 IV), HR5227 (K2 IV), HR 7560 (F8 V), and HD124570 (F8 V), with spectral types and luminosity classes similar to those of the individual components of the SZ Psc system to be used as templates in the spectral subtraction technique, and two fast rotating early-type stars, HR 8858 (B5 V, $v \sin i = 332\ \mathrm{km\ s^{-1}}$) and HR7894 (B5 IV, $v \sin i = 330\ \mathrm{km\ s^{-1}}$), to be used as a telluric water vapor line templates, were also observed with the same instrumental setup during the same observing runs.

For HiRES observations, the spectral reduction was performed with the IRAF[5] package following the standard procedures, including image trimming, bias correction, flat-field division, scattered light subtraction, 1D spectrum extraction, wavelength calibration, and spectrum continuum fitting.

[5] IRAF is distributed by the National Optical Astronomy Observatories, which is operated by the Association of Universities for Research in Astronomy (AURA), Inc., under cooperative agreement with the National Science Foundation (NSF).

Table 1
Log of the SZ Psc Observations

Date	HJD (2,450,000+)	Phase	Exp. Time (s)
2014 Oct, Xinglong 2.16 m			
2014 Oct 16	6937.0345	0.7114	1800
2014 Oct 16	6937.0602	0.7179	1800
2014 Oct 16	6937.0859	0.7244	1800
2014 Oct 16	6937.1117	0.7309	1800
2014 Oct 16	6937.1374	0.7374	1800
2014 Oct 16	6937.1631	0.7438	1800
2014 Oct 16	6937.1889	0.7503	1800
2014 Oct 16	6937.2210	0.7584	1800
2014 Oct 16	6937.2406	0.7634	1800
2015 Oct–Nov, Xinglong 2.16 m			
2015 Oct 27	7323.0463	0.0499	900
2015 Oct 27	7323.0896	0.0608	900
2015 Oct 27	7323.1024	0.0641	900
2015 Oct 27	7323.1430	0.0743	900
2015 Oct 27	7323.1558	0.0775	900
2015 Oct 27	7323.1687	0.0808	900
2015 Oct 27	7323.1815	0.0840	900
2015 Oct 28	7323.9698	0.2828	900
2015 Oct 28	7323.9826	0.2860	900
2015 Oct 28	7324.0228	0.2962	900
2015 Oct 28	7324.0356	0.2994	900
2015 Oct 28	7324.0744	0.3092	900
2015 Oct 28	7324.0872	0.3124	900
2015 Oct 28	7324.1000	0.3156	900
2015 Oct 28	7324.1128	0.3189	900
2015 Oct 28	7324.1834	0.3367	1800
2015 Oct 28	7324.2066	0.3425	1800
2015 Oct 29	7325.0540	0.5562	1800
2015 Oct 29	7325.0772	0.5620	1800
2015 Oct 29	7325.1472	0.5797	1800
2015 Oct 29	7325.1705	0.5856	1800
2015 Oct 30	7325.9413	0.7799	900
2015 Oct 30	7325.9541	0.7832	900
2015 Oct 30	7325.9934	0.7931	900
2015 Oct 30	7326.0062	0.7963	900
2015 Oct 30	7326.0447	0.8060	900
2015 Oct 30	7326.0575	0.8092	900
2015 Oct 30	7326.0963	0.8190	900
2015 Oct 30	7326.1091	0.8223	900
2015 Oct 30	7326.1491	0.8323	900
2015 Oct 30	7326.1619	0.8356	900
2015 Oct 30	7326.1747	0.8388	900
2015 Oct 30	7326.1875	0.8420	900
2015 Oct 31	7327.0451	0.0583	900
2015 Oct 31	7327.0579	0.0615	900
2015 Oct 31	7327.0965	0.0712	900
2015 Oct 31	7327.1093	0.0745	900
2015 Oct 31	7327.1484	0.0843	900
2015 Oct 31	7327.1613	0.0876	900
2015 Oct 31	7327.1742	0.0908	900
2015 Oct 31	7327.1870	0.0941	900
2015 Nov 1	7327.9399	0.2839	900
2015 Nov 1	7327.9526	0.2871	900
2015 Nov 1	7327.9911	0.2968	900
2015 Nov 1	7328.0039	0.3001	900
2015 Nov 1	7328.0424	0.3097	900
2015 Nov 1	7328.0552	0.3130	900
2015 Nov 1	7328.0937	0.3227	900
2015 Nov 1	7328.1070	0.3260	900
2015 Nov 1	7328.1455	0.3358	900
2015 Nov 1	7328.1583	0.3390	900

Table 1
(Continued)

Date	HJD (2,450,000+)	Phase	Exp. Time (s)
2015 Nov 1	7328.1711	0.3422	900
2015 Nov 1	7328.1839	0.3454	900
2015 Nov 2	7329.0172	0.5556	900
2015 Nov 2	7329.0302	0.5588	900
2015 Nov 2	7329.0690	0.5686	900
2015 Nov 2	7329.0818	0.5719	900
2015 Nov 2	7329.1204	0.5816	900
2015 Nov 2	7329.1331	0.5848	900
2015 Nov 2	7329.1719	0.5946	900
2015 Nov 2	7329.1846	0.5978	900
2015 Nov 2	7329.1974	0.6010	900
2015 Nov 2	7329.2102	0.6042	900
2016 Nov, Xinglong 2.16 m			
2016 Nov 13	7705.9716	0.6101	2400
2016 Nov 14	7706.9443	0.8554	2400
2016 Nov 14	7706.9947	0.8681	1800
2016 Nov 14	7707.0414	0.8799	1800
2016 Nov 14	7707.1078	0.8966	1800
2016 Nov 15	7707.9571	0.1108	1800
2016 Nov 15	7708.0076	0.1235	2400
2016 Nov 16	7708.9418	0.3591	1800
2016 Nov 16	7709.0962	0.3980	2400
2016 Nov 19	7711.9742	0.1238	3000
2016 Dec, Xinglong 2.16 m			
2016 Dec 16	7738.9350	0.9223	1800
2016 Dec 16	7738.9583	0.9282	1800
2016 Dec 16	7738.9986	0.9384	1800
2016 Dec 16	7739.0220	0.9443	1800
2016 Dec 17	7739.9569	0.1800	1800
2016 Dec 17	7740.0019	0.1914	1800
2016 Dec 17	7740.0253	0.1973	1800
2016 Dec 17	7740.0487	0.2032	1800
2016 Dec 18	7740.9397	0.4278	1800
2016 Dec 18	7740.9630	0.4337	1800
2016 Dec 18	7740.9864	0.4396	1800
2016 Dec 18	7741.0098	0.4455	1800
2016 Dec 18	7741.0332	0.4514	1800
2016 Dec 19	7741.9498	0.6826	1800
2016 Dec 19	7741.9732	0.6884	1800
2016 Dec 19	7742.0182	0.6998	1500
2016 Dec 19	7742.0381	0.7048	1500
2016 Dec 19	7742.0580	0.7098	1500
2017 Nov–Dec, Xinglong 2.16 m			
2017 Nov 28	8085.9639	0.4307	1800
2017 Nov 28	8085.9895	0.4372	1800
2017 Nov 28	8086.0150	0.4436	1800
2017 Nov 28	8086.0406	0.4501	1800
2017 Nov 29	8086.9536	0.6803	900
2017 Nov 29	8086.9663	0.6835	900
2017 Nov 29	8086.9792	0.6867	900
2017 Nov 29	8086.9919	0.6900	900
2017 Nov 29	8087.0047	0.6932	900
2017 Nov 29	8087.0175	0.6964	900
2017 Nov 29	8087.0303	0.6997	900
2017 Nov 29	8087.0431	0.7029	900
2017 Nov 29	8087.0559	0.7061	900
2017 Nov 29	8087.0686	0.7093	900
2017 Nov 29	8087.0814	0.7125	900
2017 Nov 29	8087.0942	0.7158	900

Table 1
(Continued)

Date	HJD (2,450,000+)	Phase	Exp. Time (s)
2017 Nov 29	8087.1070	0.7190	900
2017 Nov 29	8087.1198	0.7222	900
2017 Nov 30	8087.9503	0.9316	900
2017 Nov 30	8087.9630	0.9349	900
2017 Nov 30	8087.9758	0.9381	900
2017 Nov 30	8087.9886	0.9413	900
2017 Nov 30	8088.0014	0.9445	900
2017 Nov 30	8088.0141	0.9477	900
2017 Dec 1	8088.9863	0.1929	900
2017 Dec 1	8088.9991	0.1961	900
2017 Dec 1	8089.0119	0.1993	900
2017 Dec 1	8089.0246	0.2025	900
2017 Dec 1	8089.0374	0.2058	900
2017 Dec 1	8089.0502	0.2090	900
2017 Dec 1	8089.0630	0.2122	900
2017 Dec 1	8089.0757	0.2154	900
2017 Dec 1	8089.0885	0.2186	900
2017 Dec 1	8089.1013	0.2219	900
2017 Dec 1	8089.1140	0.2251	900
2017 Dec 5	8092.9513	0.1927	900
2017 Dec 5	8092.9641	0.1959	900
2017 Dec 5	8092.9769	0.1992	900
2017 Dec 5	8092.9896	0.2024	900
2017 Dec 5	8093.0024	0.2056	900
2017 Dec 5	8093.0152	0.2088	900
2017 Dec 5	8093.0280	0.2120	900
2017 Dec 5	8093.0407	0.2153	900
2017 Dec 5	8093.0536	0.2185	900
2017 Dec 5	8093.0665	0.2218	900
2017 Dec 5	8093.0793	0.2250	900
2017 Dec 5	8093.0927	0.2284	900
2017 Dec 5	8093.1056	0.2316	900
2017 Dec 5	8093.1183	0.2348	900
2017 Dec 6	8093.9399	0.4420	900
2017 Dec 6	8093.9526	0.4452	900
2017 Dec 6	8093.9655	0.4484	900
2017 Dec 6	8093.9782	0.4517	900
2017 Dec 7	8094.9617	0.6997	1800
2017 Dec 7	8094.9873	0.7061	1800
2017 Dec 7	8095.0129	0.7126	1800
2017 Dec 7	8095.0384	0.7190	1800
2017 Dec 7	8095.0652	0.7258	1800
2017 Dec 7	8095.0907	0.7322	1800
2017 Dec 7	8095.1163	0.7386	1800
2017 Dec 8	8095.9481	0.9484	900
2017 Dec 9	8096.9554	0.2024	1800
2017 Dec 9	8096.9886	0.2108	1800
2017 Dec 9	8097.0217	0.2191	1800
2017 Dec 9	8097.0825	0.2345	1800
2017 Dec 9	8097.1081	0.2409	1800
2017 Dec 11	8098.9470	0.7046	1800
2017 Dec 11	8098.9726	0.7111	1800
2017 Dec 11	8098.9982	0.7175	1800
2017 Dec 11	8099.0238	0.7240	1800
2017 Dec 11	8099.0494	0.7304	1800
2017 Dec 11	8099.0749	0.7369	1800
2017 Nov, Lijiang 2.4 m			
2017 Nov 1	8059.0844	0.6527	900
2017 Nov 1	8059.0975	0.6560	900
2017 Nov 1	8059.1101	0.6592	900
2017 Nov 1	8059.1227	0.6623	900
2017 Nov 1	8059.1355	0.6656	900

Table 1
(Continued)

Date	HJD (2,450,000+)	Phase	Exp. Time (s)
2017 Nov 1	8059.1483	0.6688	900
2017 Nov 2	8060.0292	0.8909	900
2017 Nov 2	8060.0418	0.8940	900
2017 Nov 2	8060.0543	0.8973	900
2017 Nov 2	8060.0668	0.9004	900
2017 Nov 2	8060.0794	0.9036	900
2017 Nov 2	8060.0921	0.9068	900
2017 Nov 2	8060.1466	0.9205	1800
2017 Nov 3	8061.1231	0.1668	900
2017 Nov 4	8062.0364	0.3971	1800
2017 Nov 4	8062.0729	0.4063	1800
2017 Nov 4	8062.0980	0.4126	1800
2017 Nov 4	8062.1231	0.4189	1800
2017 Nov 4	8062.1485	0.4253	1800
2018 Nov, Lijiang 2.4 m			
2018 Nov 21	8444.0112	0.7176	1800
2018 Nov 21	8444.0376	0.7242	1800
2018 Nov 21	8444.0704	0.7325	1800
2018 Nov 21	8444.0956	0.7389	1800
2018 Nov 21	8444.1191	0.7448	1800
2018 Nov 21	8444.1427	0.7508	1800
2018 Nov 23	8445.9850	0.2153	1800
2018 Nov 23	8446.0089	0.2213	1800
2018 Nov 23	8446.0327	0.2274	1800
2018 Nov 23	8446.0565	0.2333	1800
2018 Nov 23	8446.0825	0.2399	1800
2018 Nov 23	8446.1065	0.2460	1800
2018 Nov 23	8446.1305	0.2520	1800
2018 Nov 23	8446.1540	0.2579	1800
2018 Nov 25	8447.9733	0.7167	1800
2018 Nov 25	8447.9973	0.7227	1800
2018 Nov 25	8448.0208	0.7287	1800
2018 Nov 25	8448.0443	0.7346	1800
2018 Nov 25	8448.0678	0.7405	1800
2018 Nov 25	8448.0914	0.7465	1800
2018 Nov 25	8448.1161	0.7527	1800
2018 Aug, TIGRE 1.2 m			
2018 Aug 22	8352.7357	0.7011	810
2018 Aug 24	8354.8769	0.2411	1800
2018 Aug 28	8358.7448	0.2164	1800
2018 Nov, TIGRE 1.2 m			
2018 Nov 24	8446.5443	0.3564	1800
2018 Nov 25	8447.5445	0.6086	1800
2018 Nov 27	8449.5440	0.1128	1800

(This table is available in its entirety in machine-readable form.)

The wavelength calibration was obtained using a lot of the emission lines of a Th–Ar lamp, and all spectra were normalized using a low-order polynomial fit to the observed continuum. TIGRE observations were fully automatic reduced with the spectral reduction pipeline (Mittag et al. 2010), which includes all standard and necessary reduction steps for echelle spectra. For the extracted and wavelength-calibrated spectra derived by the pipeline, we normalized them using a low-order polynomial fit to the observed continuum in the IRAF package. Finally, for some of our observations during which the telluric absorption lines were very heavy, we eliminated the telluric water vapor lines in the chromospheric activity line regions of interest using the spectra of HR 8858 and HR7894 with an interactive procedure in the IRAF package for HiRES and TIGRE observations, respectively. Examples of removing the telluric absorption lines in different spectral regions can be seen in Gu et al. (2002) in detail.

In Figure 1, we display examples of the normalized Ca II IRT, H_α, Na I D_1, D_2 doublet, He I D_3, and H_β line profiles of the SZ Psc system obtained at phase 0.296 in 2015 October 28. Because the signal-to-noise ratio (S/N) is very low in the Ca II H & K line regions for HiRES observations, we give an example of these two lines obtained by TIGRE observations in Figure 2.

3. Chromospheric Activity

3.1. Chromospheric Activity Indicators

Optical chromospheric activity indicators Ca II IRT, H_α, Na I D_1, D_2 doublet, He I D_3, H_β, and Ca II H & K lines, formed at different atmospheric heights from the region of the temperature minimum to the upper chromosphere, are simultaneously studied in the present work. To extract the activity signatures from the photosphere absorption profile in these indicator lines, we use the spectral subtraction technique for all the observed spectra with the help of the popular program STARMOD (Barden 1985; Montes et al. 1995a, 1995b, 1997, 2000), which has been widely used for chromospheric activity studies and prominence detection.

Due to the very weak spectral signal of the tertiary component in the SZ Psc system, it is not necessary to consider its contribution to the total system during the spectral analysis. For HiRES observations, we respectively use spectra of two inactive stars, HR 7690 and HR 7560, as templates for the K1 IV primary and F8 V secondary star to construct the synthesized spectra representing the non-active state of the SZ Psc system. The rotational velocity ($v \sin i$) values of 78 km s^{-1} for the primary star and 2 km s^{-1} for the secondary component are taken from C19, and the adopted intensity weight ratios, derived from high S/N spectra at phases where the two components of the system were well separated, are 0.83/0.17 for the Ca II IRT spectral region, 0.815/0.185 for the H_α spectral region, 0.775/0.225 for the Na I D_1, D_2 doublet, He I D_3 spectral region, and 0.70/0.30 for the H_β spectral region. Consequently, the synthesized spectra in all the observations are constructed by broadening and weighting the template spectra to the above derived values, and shifting along radial-velocity axis. Finally, the subtracted spectra between the observed and the synthesized spectra are obtained, which present activity contribution as excess emission or absorption features for the SZ Psc system.

Due to the template stars used for HiRES, spectra were not obtained for the TIGRE observations; we use spectra of the other two inactive stars HR 5227 and HD 124570 as templates for the primary and secondary star of the SZ Psc system, and then the same $v \sin i$ values and intensity weight ratios in different spectra line regions as HiRES observations are also adopted for the Ca II IRT (λ8662, λ8542, and λ8498), H_α, and H_β line spectral regions in the courses of the synthesized spectra construction.

Examples of the spectral subtraction in the Ca II IRT, H_α, Na I D_1, D_2 doublet, He I D_3, and H_β line spectral regions are also presented in Figure 1, in which it could be found that the

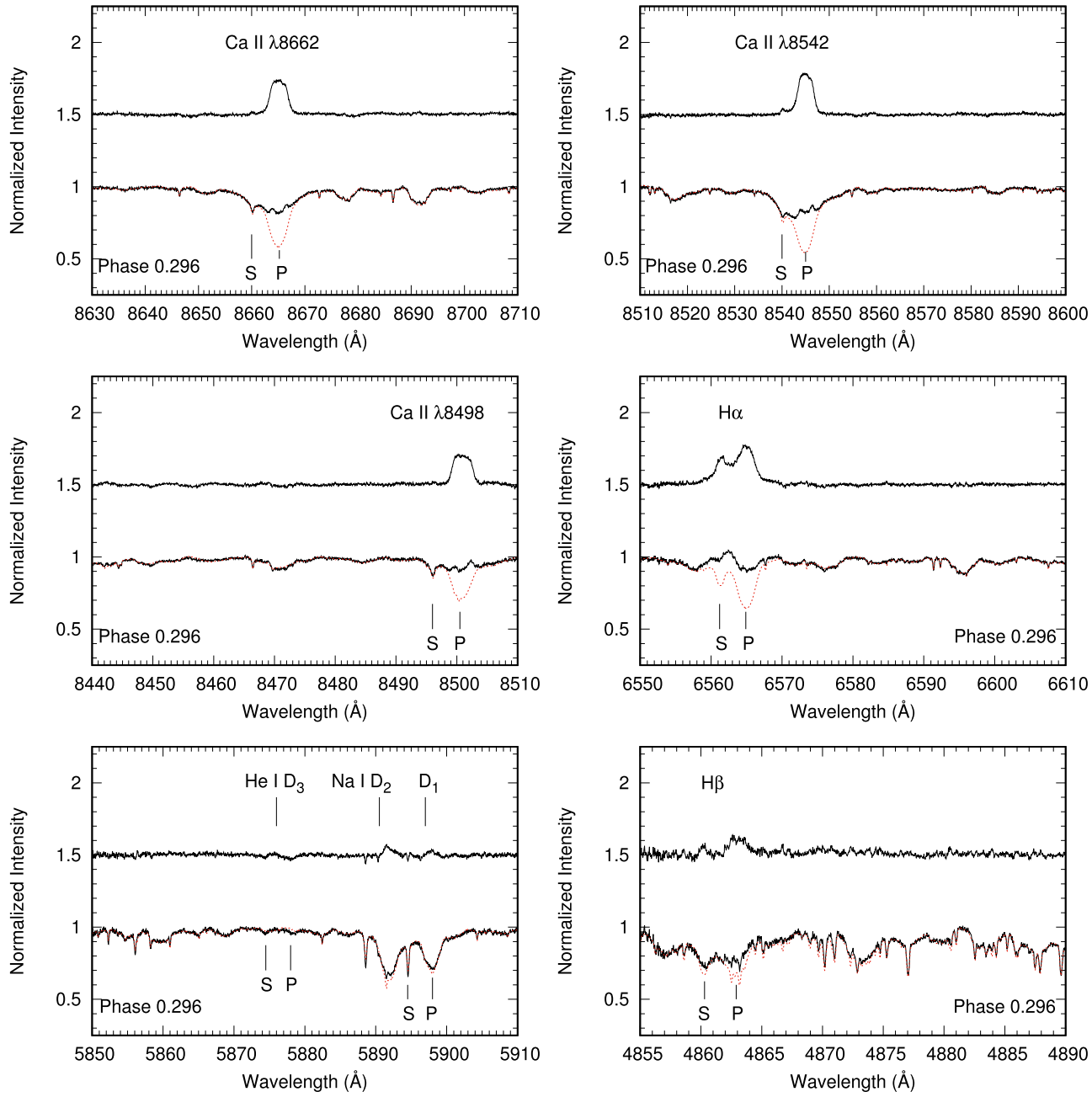

Figure 1. Examples of the observed, synthesized, and subtracted spectra for the Ca II IRT (λ8662, λ8542, and λ8498), H_α, Na I D_1, D_2 doublet, He I D_3, and H_β line spectral regions. For each panel, the lower solid line is the observed spectrum, the dotted line represents the synthesized spectrum, and the upper spectrum is the subtracted one, shifted for better display. "P" and "S" indicate the primary and secondary components of the SZ Psc system, respectively.

synthesized spectra match the observational ones well. After applying the spectral subtraction technique, we can see that the Ca II IRT, H_α, Na I D_1, D_2 doublet, and H_β lines show excess emission in the subtraction and the emission mainly associated with the active chromosphere of the K1 IV primary star of the SZ Psc system, which is in good agreement with the previous findings in the chromospheric activity lines Mg II h & k, Ca II H & K, H_α, and Ca II IRT. However, for some of our observations, it is also seen that some evidence of excess emission from the F8 V secondary present in the subtraction, especially for the H_α line, which means that the F8 V star is also active in the SZ Psc system. About the activity of the F8 V star, Huenemoerder & Ramsey (1984) found that there seem to be some excess emission feature in the H_α line from this star near orbital phase 0.75 during their observations. Moreover, Lanza et al. (2001) derived the starspot distribution over the surface of the F8 V star based on a long-term sequence of *V*-band light curves and Oláh (2006) also concluded that the SZ Psc system has starspot activity on both components. Therefore, all these observing facts indicate that the F8 V secondary is also active in the SZ Psc system, but less active.

For the Ca II H & K lines, as shown in Figure 2, more clear and strong emission features appear, which also indicate the active chromosphere of the K1 IV primary star of the SZ Psc system.

Different from the behavior of these chromospheric activity indicators, as shown in Figure 1, the He I D_3 line usually exhibits a very weak absorption feature in the subtraction for

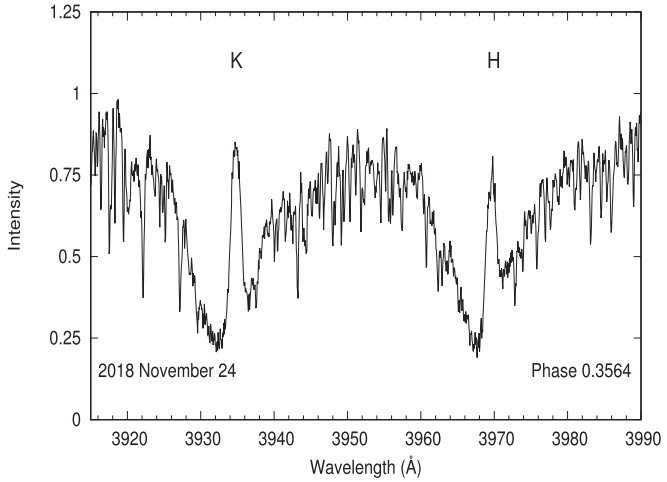

Figure 2. Example of the Ca II H & K lines obtained by TIGRE observations.

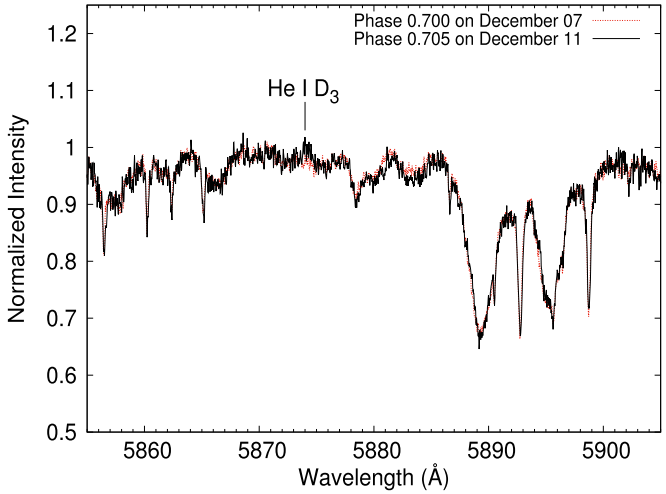

Figure 3. Comparing the He I D_3 line of SZ Psc observed at the similar orbital phase between the flare (solid line) and quiescent state (dotted line).

both components of the SZ Psc system. Possibly because the He I D_3 line is very weak, the absorption feature in this line was easily neglected in the previous literatures for this system. Actually, the He I D_3 line in weak absorption has also been found in several RS CVn-type systems (Montes et al. 1997, 2000).

The equivalent widths (EWs) of the subtracted Ca II IRT, H_α, and H_β lines were measured using the SPLOT task in the IRAF package, following the methods described in our previous papers (Cao & Gu 2014, 2015, 2017), and are listed in Table 2 along with their errors. For some of our observations, because the S/Ns are very low in the H_β line region, they were not included in the analysis. In Table 2, we also give the ratios of excess emission, EW_{8542}/EW_{8498}, which are in the range of 1–2. The values are consistent with the ratios for several other chromospheric activity stars (e.g., Montes et al. 2000; Gu et al. 2002; López-Santiago et al. 2003; Gálvez et al. 2009; Cao & Gu 2014, 2015, 2017; Zhang et al. 2016) and for the SZ Psc system derived by Zhang & Gu (2008) and in C19, which indicate that the Ca II IRT line emission probably arises from plage-like regions.

3.2. Optical Flare Event

Due to its very high excitation potential, emission in the He I D_3 line is indicative for flares in the optical spectral range, as observed during flare events in the Sun (Tandberg-Hanssen 1967; Zirin 1988) and in several active RS CVn-type systems, such as II Peg (Huenemoerder & Ramsey 1987; Montes et al. 1997; Berdyugina et al. 1999; Gu & Tan 2003; Frasca et al. 2008), V711 Tau (Cao & Gu 2015), UX Ari (Montes et al. 1996; Gu et al. 2002; Cao & Gu 2017), and DM UMa (Zhang et al. 2016). For the SZ Psc system, a strong optical two-ribbon flare event characterized by the obvious He I D_3 line emission as well as a stronger emission feature in the H_α line and the other chromospheric activity lines, was detected in C19. Moreover, it is noticeable that the gradual decay of this strong optical flare was accompanied by the appearance of cool post-flare loops presented as a fast evolved absorption feature in the blue wing of the chromospheric H_α emission profile, which is a very unusual magnetic activity event in the stellar case.

During our observations of 2017 December 11 near the second quadrature of the system, an optical flare was detected, which is characterized by the prominent He I D_3 line emission feature, as an example displayed in Figure 3 where we compare the He I D_3 line profile with the one derived at the similar orbital phase but in the previous orbital cycle (assumed in a quiescent state). Moreover, the other chromospheric activity indicators also show dramatic increased emission during the flare event. In Figure 4, we show the H_α line profiles during the flare and in a quiescent state, which reveals a much stronger emission feature in the observed and subtracted spectra during the flare.

Calculating the stellar continuum flux F_{H_α} (erg cm^{-2} s^{-1} Å^{-1}) in the H_α line as a function of the color index ($B-V$) ($\sim$0.846 for SZ Psc; see Messina 2008) based on the calibration of Hall (1996) and then converting the EW into the absolute surface fluxes F_S (erg cm^{-2} s^{-1}), we have estimated the flare energy $E = 4\pi\ {R_*}^2\ F_S \simeq 2.48 \times 10^{31}$ erg s^{-1} in the H_α line at phase 0.7049. The radius $R_* = 6.0\ R_\odot$ of the K1 IV primary star (Eaton & Henry 2007) is used for the calculation. Because the K1 IV star is very active in the SZ Psc system and the flare enhancements are mainly associated with this component (see Figure 4), we have assumed that the flare happened on this star. We have also corrected the EWs to the total continuum before they are converted to the absolute flux at the stellar surface. The value of this optical flare for energy released in the H_α line has a similar order of magnitude to the ones for the other RS CVn-type stars (Catalano & Frasca 1994; Montes et al. 1996; Gu et al. 2002; García-Alvarez et al. 2003; Cao & Gu 2015, 2017) and the previous optical flare for the SZ Psc system (see C19 for a detailed description) but much weaker.

3.3. Chromospheric Activity Variation

For the SZ Psc system, the chromospheric excess H_α emission derived by Huenemoerder & Ramsey (1984) showed large intrinsic scatter and no systematic variability behavior with the orbital phase. Moreover, Eaton & Henry (2007) also found that the variability of chromospheric H_α emission seems independent of the orbital phase on average, but it could increase markedly for periods of a few orbital cycles. However, Kang et al. (2003) investigated the Mg II h and k emission lines of the SZ Psc system, and concluded that the intensity variation of the emission line is correlated with the orbital phase.

Table 2
Measurements for the Subtraction Profiles of the Ca II λ8662, Ca II λ8542, λ8498, H_α, and H_β Lines, and values of EW(λ8542)/EW(λ8498)

HJD (2,450,000+)	Phase	EW(Å)					$\frac{EW(\lambda8542)}{EW(\lambda8498)}$
		Ca II λ8662	Ca II λ8542	Ca II λ8498	H_α	H_β	
			2014 Oct				
6937.0345	0.7114	0.738 ± 0.003	0.884 ± 0.005	0.548 ± 0.004	0.626 ± 0.011	···	1.61
6937.0602	0.7179	0.776 ± 0.007	0.902 ± 0.022	0.596 ± 0.007	0.732 ± 0.030	···	1.51
6937.0859	0.7244	0.780 ± 0.004	0.901 ± 0.021	0.588 ± 0.009	0.646 ± 0.026	···	1.53
6937.1117	0.7309	0.767 ± 0.007	0.885 ± 0.008	0.589 ± 0.005	0.526 ± 0.011	···	1.50
6937.1374	0.7374	0.769 ± 0.017	0.892 ± 0.010	0.606 ± 0.009	0.479 ± 0.014	···	1.47
6937.1631	0.7438	0.788 ± 0.009	0.877 ± 0.030	0.575 ± 0.007	0.392 ± 0.019	···	1.53
6937.1889	0.7503	0.786 ± 0.009	0.903 ± 0.012	0.584 ± 0.014	0.482 ± 0.013	···	1.55
6937.2210	0.7584	0.785 ± 0.010	0.908 ± 0.012	0.604 ± 0.006	0.527 ± 0.013	···	1.60
6937.2406	0.7634	0.800 ± 0.008	0.923 ± 0.011	0.591 ± 0.005	0.526 ± 0.012	···	1.56
			2015 Oct–Dec				
7323.0463	0.0499	0.871 ± 0.034	1.115 ± 0.011	0.689 ± 0.011	1.320 ± 0.010	0.181 ± 0.019	1.62
7323.0896	0.0608	0.855 ± 0.016	1.134 ± 0.006	0.684 ± 0.012	1.397 ± 0.011	0.178 ± 0.014	1.66
7323.1024	0.0641	0.851 ± 0.009	1.114 ± 0.012	0.683 ± 0.011	1.387 ± 0.013	0.184 ± 0.020	1.63
7323.1430	0.0743	0.855 ± 0.010	1.106 ± 0.014	0.673 ± 0.008	1.360 ± 0.011	0.156 ± 0.015	1.64
7323.1558	0.0775	0.848 ± 0.006	1.094 ± 0.013	0.680 ± 0.015	1.324 ± 0.012	0.186 ± 0.018	1.61
7323.1687	0.0808	0.850 ± 0.015	1.114 ± 0.014	0.691 ± 0.012	1.284 ± 0.016	0.183 ± 0.016	1.61
7323.1815	0.0840	0.851 ± 0.006	1.115 ± 0.011	0.685 ± 0.018	1.243 ± 0.011	0.159 ± 0.014	1.63
7323.9698	0.2828	0.886 ± 0.014	1.133 ± 0.012	0.727 ± 0.013	1.389 ± 0.009	0.284 ± 0.017	1.56
7323.9826	0.2860	0.891 ± 0.016	1.192 ± 0.012	0.731 ± 0.014	1.387 ± 0.010	0.277 ± 0.013	1.63
7324.0228	0.2962	0.892 ± 0.029	1.125 ± 0.013	0.727 ± 0.016	1.332 ± 0.013	0.260 ± 0.016	1.55
7324.0356	0.2994	0.873 ± 0.021	1.130 ± 0.013	0.724 ± 0.013	1.373 ± 0.011	0.212 ± 0.014	1.56
7324.0744	0.3092	0.880 ± 0.032	1.135 ± 0.008	0.708 ± 0.012	1.351 ± 0.017	0.203 ± 0.012	1.60
7324.0872	0.3124	0.867 ± 0.029	1.123 ± 0.014	0.706 ± 0.014	1.319 ± 0.015	0.181 ± 0.016	1.59
7324.1000	0.3156	0.872 ± 0.023	1.123 ± 0.018	0.707 ± 0.009	1.324 ± 0.016	0.216 ± 0.015	1.59
7324.1128	0.3189	0.868 ± 0.024	1.115 ± 0.014	0.700 ± 0.011	1.326 ± 0.011	0.225 ± 0.019	1.59
7324.1834	0.3367	0.863 ± 0.026	1.110 ± 0.014	0.700 ± 0.014	1.334 ± 0.021	0.174 ± 0.017	1.59
7324.2066	0.3425	0.864 ± 0.020	1.110 ± 0.012	0.684 ± 0.011	1.244 ± 0.013	0.176 ± 0.020	1.62
7325.0540	0.5562	0.783 ± 0.012	0.920 ± 0.014	0.631 ± 0.011	0.937 ± 0.015	···	1.46
7325.0772	0.5620	0.789 ± 0.013	0.949 ± 0.017	0.614 ± 0.007	0.956 ± 0.014	···	1.55
7325.1472	0.5797	0.786 ± 0.010	0.924 ± 0.008	0.623 ± 0.012	0.944 ± 0.017	···	1.48
7325.1705	0.5856	0.777 ± 0.009	0.920 ± 0.007	0.623 ± 0.016	0.856 ± 0.012	···	1.48
7325.9413	0.7799	0.760 ± 0.011	0.900 ± 0.013	0.622 ± 0.013	1.164 ± 0.009	−0.051 ± 0.012	1.45
7325.9541	0.7832	0.760 ± 0.013	0.884 ± 0.015	0.612 ± 0.010	1.050 ± 0.010	−0.080 ± 0.014	1.44
7325.9934	0.7931	0.760 ± 0.010	0.888 ± 0.010	0.618 ± 0.012	1.143 ± 0.011	−0.105 ± 0.016	1.44
7326.0062	0.7963	0.767 ± 0.012	0.917 ± 0.010	0.613 ± 0.012	1.112 ± 0.007	−0.098 ± 0.013	1.50
7326.0447	0.8060	0.774 ± 0.013	0.898 ± 0.013	0.627 ± 0.012	1.167 ± 0.010	−0.106 ± 0.017	1.43
7326.0575	0.8092	0.759 ± 0.015	0.892 ± 0.015	0.616 ± 0.014	1.156 ± 0.009	−0.068 ± 0.019	1.45
7326.0963	0.8190	0.764 ± 0.011	0.875 ± 0.011	0.632 ± 0.013	1.126 ± 0.010	−0.058 ± 0.016	1.38
7326.1091	0.8223	0.758 ± 0.010	0.905 ± 0.012	0.641 ± 0.011	1.128 ± 0.012	−0.069 ± 0.015	1.41
7326.1491	0.8323	0.774 ± 0.012	0.922 ± 0.011	0.629 ± 0.015	1.272 ± 0.008	−0.072 ± 0.012	1.47
7326.1619	0.8356	0.773 ± 0.009	0.894 ± 0.008	0.637 ± 0.014	1.293 ± 0.013	−0.090 ± 0.015	1.40
7326.1747	0.8388	0.768 ± 0.011	0.923 ± 0.011	0.653 ± 0.014	1.293 ± 0.011	−0.070 ± 0.013	1.41
7326.1875	0.8420	0.791 ± 0.013	0.910 ± 0.014	0.638 ± 0.015	1.154 ± 0.010	−0.087 ± 0.011	1.43
7327.0451	0.0583	0.862 ± 0.018	1.148 ± 0.013	0.699 ± 0.013	1.650 ± 0.018	0.245 ± 0.017	1.64
7327.0579	0.0615	0.887 ± 0.021	1.192 ± 0.012	0.713 ± 0.014	1.721 ± 0.014	0.251 ± 0.015	1.67
7327.0965	0.0712	0.927 ± 0.019	1.229 ± 0.016	0.741 ± 0.012	1.772 ± 0.021	0.302 ± 0.019	1.66
7327.1093	0.0745	0.929 ± 0.017	1.229 ± 0.012	0.739 ± 0.012	1.768 ± 0.011	0.313 ± 0.018	1.66
7327.1484	0.0843	0.933 ± 0.022	1.229 ± 0.011	0.749 ± 0.013	1.669 ± 0.015	0.262 ± 0.023	1.64
7327.1613	0.0876	0.926 ± 0.018	1.211 ± 0.010	0.755 ± 0.013	1.621 ± 0.013	0.263 ± 0.019	1.60
7327.1742	0.0908	0.926 ± 0.019	1.198 ± 0.012	0.740 ± 0.014	1.605 ± 0.018	0.270 ± 0.013	1.62
7327.1870	0.0941	0.922 ± 0.021	1.226 ± 0.013	0.751 ± 0.016	1.617 ± 0.017	0.242 ± 0.017	1.63
7327.9399	0.2839	0.853 ± 0.019	1.167 ± 0.015	0.694 ± 0.012	1.665 ± 0.019	0.225 ± 0.020	1.68
7327.9526	0.2871	0.875 ± 0.012	1.165 ± 0.012	0.692 ± 0.010	1.615 ± 0.014	0.243 ± 0.016	1.68
7327.9911	0.2968	0.883 ± 0.012	1.152 ± 0.014	0.697 ± 0.009	1.585 ± 0.021	0.259 ± 0.014	1.65
7328.0039	0.3001	0.885 ± 0.008	1.169 ± 0.016	0.698 ± 0.011	1.605 ± 0.011	0.236 ± 0.018	1.67
7328.0424	0.3097	0.864 ± 0.009	1.175 ± 0.007	0.682 ± 0.012	1.595 ± 0.013	0.262 ± 0.011	1.72
7328.0552	0.3130	0.858 ± 0.013	1.157 ± 0.010	0.691 ± 0.011	1.526 ± 0.016	0.242 ± 0.016	1.67
7328.0937	0.3227	0.871 ± 0.012	1.133 ± 0.012	0.703 ± 0.015	1.512 ± 0.015	0.214 ± 0.013	1.61
7328.1070	0.3260	0.865 ± 0.034	1.128 ± 0.011	0.697 ± 0.013	1.506 ± 0.011	0.206 ± 0.015	1.62
7328.1455	0.3358	0.892 ± 0.020	1.177 ± 0.013	0.698 ± 0.014	1.401 ± 0.010	0.233 ± 0.017	1.69
7328.1583	0.3390	0.900 ± 0.010	1.167 ± 0.011	0.702 ± 0.012	1.412 ± 0.014	0.242 ± 0.012	1.66

Table 2
(Continued)

HJD (2,450,000+)	Phase	EW(Å)					$\frac{EW(\lambda8542)}{EW(\lambda8498)}$
		Ca II λ8662	Ca II λ8542	Ca II λ8498	H_α	H_β	
7328.1711	0.3422	0.884 ± 0.021	1.164 ± 0.018	0.709 ± 0.011	1.418 ± 0.011	0.204 ± 0.014	1.64
7328.1839	0.3454	0.869 ± 0.013	1.143 ± 0.012	0.696 ± 0.008	1.395 ± 0.021	0.206 ± 0.011	1.64
7329.0172	0.5556	0.838 ± 0.021	0.990 ± 0.016	0.631 ± 0.012	1.168 ± 0.013	−0.164 ± 0.013	1.57
7329.0302	0.5588	0.839 ± 0.013	0.990 ± 0.015	0.633 ± 0.008	1.248 ± 0.017	−0.141 ± 0.016	1.56
7329.0690	0.5686	0.831 ± 0.024	0.938 ± 0.010	0.619 ± 0.015	1.316 ± 0.021	−0.112 ± 0.019	1.52
7329.0818	0.5719	0.814 ± 0.020	0.938 ± 0.016	0.616 ± 0.011	1.390 ± 0.011	−0.065 ± 0.014	1.52
7329.1204	0.5816	0.807 ± 0.013	0.980 ± 0.011	0.607 ± 0.011	1.395 ± 0.013	−0.077 ± 0.018	1.61
7329.1331	0.5848	0.807 ± 0.008	0.983 ± 0.016	0.614 ± 0.012	1.413 ± 0.008	−0.070 ± 0.015	1.60
7329.1719	0.5946	0.825 ± 0.014	1.002 ± 0.013	0.621 ± 0.012	1.480 ± 0.015	−0.021 ± 0.021	1.61
7329.1846	0.5978	0.820 ± 0.008	0.989 ± 0.014	0.622 ± 0.015	1.550 ± 0.017	−0.023 ± 0.017	1.59
7329.1974	0.6010	0.814 ± 0.017	1.009 ± 0.012	0.612 ± 0.012	1.528 ± 0.013	−0.040 ± 0.013	1.65
7329.2102	0.6042	0.824 ± 0.012	0.988 ± 0.012	0.613 ± 0.013	1.491 ± 0.016	−0.032 ± 0.016	1.61
			2016 Nov				
7705.9716	0.6101	0.875 ± 0.015	1.059 ± 0.017	0.680 ± 0.006	1.423 ± 0.013	0.062 ± 0.030	1.56
7706.9443	0.8554	0.762 ± 0.013	1.005 ± 0.018	0.684 ± 0.014	0.980 ± 0.048	−0.113 ± 0.031	1.47
7706.9947	0.8681	0.743 ± 0.012	1.014 ± 0.022	0.686 ± 0.011	0.978 ± 0.050	−0.127 ± 0.019	1.48
7707.0414	0.8799	0.737 ± 0.017	1.005 ± 0.028	0.669 ± 0.010	0.947 ± 0.060	−0.126 ± 0.021	1.50
7707.1078	0.8966	0.760 ± 0.015	0.996 ± 0.023	0.662 ± 0.010	0.925 ± 0.046	−0.084 ± 0.020	1.50
7707.9571	0.1108	0.813 ± 0.012	1.155 ± 0.015	0.690 ± 0.020	1.571 ± 0.021	0.152 ± 0.016	1.67
7708.0076	0.1235	0.856 ± 0.035	1.230 ± 0.017	0.727 ± 0.011	1.692 ± 0.024	0.214 ± 0.014	1.69
7708.9418	0.3591	1.004 ± 0.018	1.303 ± 0.011	0.816 ± 0.015	2.081 ± 0.015	0.307 ± 0.017	1.60
7709.0962	0.3980	1.030 ± 0.012	1.364 ± 0.013	0.853 ± 0.013	2.100 ± 0.021	0.286 ± 0.012	1.60
7711.9742	0.1238	0.836 ± 0.013	1.027 ± 0.014	0.667 ± 0.010	1.193 ± 0.021	−0.193 ± 0.020	1.54
			2016 Dec				
7738.9350	0.9223	0.872 ± 0.009	1.159 ± 0.010	0.647 ± 0.010	1.294 ± 0.011	0.175 ± 0.016	1.79
7738.9583	0.9282	0.856 ± 0.011	1.125 ± 0.009	0.646 ± 0.015	1.258 ± 0.010	0.151 ± 0.013	1.74
7738.9986	0.9384	0.838 ± 0.010	1.128 ± 0.011	0.657 ± 0.013	1.244 ± 0.013	0.113 ± 0.017	1.72
7739.0220	0.9443	0.835 ± 0.023	1.109 ± 0.013	0.641 ± 0.009	1.223 ± 0.015	0.106 ± 0.019	1.73
7739.9569	0.1800	0.886 ± 0.011	1.132 ± 0.008	0.652 ± 0.006	1.317 ± 0.009	0.241 ± 0.015	1.74
7740.0019	0.1914	0.896 ± 0.018	1.132 ± 0.011	0.645 ± 0.006	1.253 ± 0.014	0.207 ± 0.016	1.76
7740.0253	0.1973	0.899 ± 0.017	1.139 ± 0.013	0.644 ± 0.013	1.207 ± 0.012	0.176 ± 0.019	1.77
7740.0487	0.2032	0.878 ± 0.020	1.122 ± 0.010	0.642 ± 0.011	1.184 ± 0.012	0.165 ± 0.017	1.75
7740.9397	0.4278	0.872 ± 0.011	1.196 ± 0.011	0.703 ± 0.013	1.070 ± 0.012	0.137 ± 0.021	1.70
7740.9630	0.4337	0.885 ± 0.013	1.191 ± 0.009	0.689 ± 0.010	0.997 ± 0.007	0.114 ± 0.019	1.73
7740.9864	0.4396	0.855 ± 0.010	1.165 ± 0.014	0.683 ± 0.012	0.943 ± 0.011	0.100 ± 0.020	1.71
7741.0098	0.4455	0.852 ± 0.012	1.164 ± 0.011	0.696 ± 0.008	0.929 ± 0.013	0.086 ± 0.023	1.67
7741.0332	0.4514	0.853 ± 0.015	1.152 ± 0.013	0.682 ± 0.010	0.908 ± 0.016	0.076 ± 0.017	1.69
7741.9498	0.6826	0.838 ± 0.010	1.093 ± 0.012	0.636 ± 0.011	1.574 ± 0.010	0.190 ± 0.019	1.72
7741.9732	0.6884	0.862 ± 0.012	1.094 ± 0.010	0.646 ± 0.090	1.571 ± 0.022	0.200 ± 0.014	1.69
7742.0182	0.6998	0.844 ± 0.008	1.076 ± 0.011	0.635 ± 0.010	1.457 ± 0.021	0.202 ± 0.017	1.69
7742.0381	0.7048	0.835 ± 0.011	1.071 ± 0.011	0.639 ± 0.013	1.451 ± 0.011	0.207 ± 0.020	1.68
7742.0580	0.7098	0.829 ± 0.009	1.080 ± 0.009	0.623 ± 0.011	1.446 ± 0.012	0.168 ± 0.019	1.73
			2017 Nov				
8059.0844	0.6527	0.931 ± 0.017	1.065 ± 0.013	0.670 ± 0.015	1.844 ± 0.009	0.170 ± 0.015	1.59
8059.0975	0.6560	0.914 ± 0.024	1.054 ± 0.021	0.645 ± 0.012	1.907 ± 0.029	0.212 ± 0.018	1.63
8059.1101	0.6592	0.924 ± 0.022	1.088 ± 0.015	0.651 ± 0.017	1.786 ± 0.014	0.288 ± 0.017	1.67
8059.1227	0.6623	0.897 ± 0.012	1.068 ± 0.018	0.645 ± 0.019	1.783 ± 0.026	0.226 ± 0.021	1.66
8059.1355	0.6656	0.914 ± 0.011	1.077 ± 0.036	0.655 ± 0.020	1.781 ± 0.036	0.230 ± 0.016	1.64
8059.1483	0.6688	0.940 ± 0.012	1.082 ± 0.030	0.676 ± 0.011	1.742 ± 0.016	0.246 ± 0.018	1.60
8060.0292	0.8909	0.931 ± 0.019	1.089 ± 0.016	0.701 ± 0.014	1.582 ± 0.030	0.019 ± 0.019	1.55
8060.0418	0.8940	0.916 ± 0.020	1.075 ± 0.018	0.704 ± 0.012	1.601 ± 0.029	0.035 ± 0.015	1.53
8060.0543	0.8973	0.927 ± 0.014	1.097 ± 0.015	0.695 ± 0.016	1.554 ± 0.008	0.030 ± 0.017	1.58
8060.0668	0.9004	0.920 ± 0.012	1.088 ± 0.012	0.680 ± 0.011	1.598 ± 0.011	0.023 ± 0.017	1.60
8060.0794	0.9036	0.917 ± 0.012	1.054 ± 0.014	0.690 ± 0.015	1.567 ± 0.020	0.038 ± 0.019	1.53
8060.0921	0.9068	0.933 ± 0.014	1.077 ± 0.012	0.696 ± 0.019	1.523 ± 0.025	0.042 ± 0.013	1.55
8060.1466	0.9205	0.976 ± 0.026	1.131 ± 0.012	0.699 ± 0.020	1.623 ± 0.011	0.100 ± 0.016	1.62
8061.1231	0.1668	0.903 ± 0.018	1.202 ± 0.020	0.739 ± 0.027	1.766 ± 0.044	0.085 ± 0.020	1.63
8062.0364	0.3971	0.964 ± 0.011	1.334 ± 0.016	0.841 ± 0.020	1.245 ± 0.011	0.059 ± 0.017	1.59
8062.0729	0.4063	0.938 ± 0.012	1.273 ± 0.014	0.768 ± 0.026	1.227 ± 0.014	0.074 ± 0.022	1.66
8062.0980	0.4126	0.966 ± 0.021	1.292 ± 0.018	0.789 ± 0.018	1.281 ± 0.014	0.088 ± 0.019	1.64
8062.1231	0.4189	0.967 ± 0.016	1.305 ± 0.017	0.743 ± 0.013	1.323 ± 0.020	0.092 ± 0.020	1.76

Table 2
(Continued)

HJD (2,450,000+)	Phase	EW(Å)					$\frac{EW(\lambda8542)}{EW(\lambda8498)}$
		Ca II $\lambda8662$	Ca II $\lambda8542$	Ca II $\lambda8498$	H_α	H_β	
8062.1485	0.4253	0.954 ± 0.012	1.306 ± 0.015	0.772 ± 0.021	1.335 ± 0.025	0.082 ± 0.017	1.69
			2017 Nov–Dec				
8085.9639	0.4307	0.917 ± 0.017	1.167 ± 0.020	0.646 ± 0.021	0.779 ± 0.010	⋯	1.81
8085.9895	0.4372	0.898 ± 0.015	1.182 ± 0.022	0.683 ± 0.015	0.766 ± 0.015	⋯	1.73
8086.0150	0.4436	0.889 ± 0.020	1.128 ± 0.022	0.661 ± 0.019	0.739 ± 0.012	⋯	1.71
8086.0406	0.4501	0.936 ± 0.016	1.211 ± 0.028	0.632 ± 0.012	0.805 ± 0.011	⋯	1.92
8086.9536	0.6803	0.860 ± 0.019	1.157 ± 0.019	0.640 ± 0.016	1.462 ± 0.011	0.176 ± 0.021	1.81
8086.9663	0.6835	0.899 ± 0.013	1.176 ± 0.021	0.624 ± 0.015	1.437 ± 0.014	0.183 ± 0.018	1.88
8086.9792	0.6867	0.884 ± 0.017	1.131 ± 0.018	0.597 ± 0.011	1.478 ± 0.011	0.210 ± 0.019	1.89
8086.9919	0.6900	0.886 ± 0.016	1.101 ± 0.019	0.615 ± 0.012	1.439 ± 0.016	0.201 ± 0.020	1.79
8087.0047	0.6932	0.871 ± 0.021	1.120 ± 0.023	0.632 ± 0.018	1.476 ± 0.012	0.201 ± 0.017	1.77
8087.0175	0.6964	0.885 ± 0.015	1.129 ± 0.021	0.606 ± 0.011	1.498 ± 0.011	0.193 ± 0.015	1.86
8087.0303	0.6997	0.896 ± 0.013	1.171 ± 0.020	0.601 ± 0.014	1.401 ± 0.016	0.202 ± 0.019	1.95
8087.0431	0.7029	0.872 ± 0.019	1.112 ± 0.018	0.610 ± 0.012	1.322 ± 0.016	0.196 ± 0.013	1.82
8087.0559	0.7061	0.867 ± 0.017	1.083 ± 0.021	0.607 ± 0.016	1.539 ± 0.023	0.194 ± 0.011	1.78
8087.0686	0.7093	0.906 ± 0.020	1.100 ± 0.023	0.613 ± 0.019	1.397 ± 0.014	0.188 ± 0.016	1.79
8087.0814	0.7125	0.881 ± 0.018	1.141 ± 0.022	0.618 ± 0.021	1.305 ± 0.011	0.189 ± 0.014	1.85
8087.0942	0.7158	0.896 ± 0.025	1.128 ± 0.020	0.564 ± 0.016	1.203 ± 0.012	0.186 ± 0.012	2.00
8087.1070	0.7190	0.879 ± 0.022	1.155 ± 0.019	0.585 ± 0.014	1.196 ± 0.014	0.185 ± 0.015	1.97
8087.1198	0.7222	0.887 ± 0.015	1.177 ± 0.023	0.576 ± 0.017	1.405 ± 0.022	0.183 ± 0.016	2.04
8087.9503	0.9316	0.935 ± 0.018	1.303 ± 0.019	0.668 ± 0.023	1.191 ± 0.009	⋯	1.95
8087.9630	0.9349	0.922 ± 0.014	1.293 ± 0.017	0.667 ± 0.020	1.176 ± 0.020	⋯	1.94
8087.9758	0.9381	0.913 ± 0.017	1.249 ± 0.019	0.656 ± 0.018	1.139 ± 0.014	⋯	1.90
8087.9886	0.9413	0.921 ± 0.019	1.285 ± 0.021	0.676 ± 0.022	1.041 ± 0.021	⋯	1.90
8088.0014	0.9445	0.946 ± 0.022	1.301 ± 0.017	0.686 ± 0.017	1.135 ± 0.011	⋯	1.90
8088.0141	0.9477	0.937 ± 0.018	1.329 ± 0.020	0.654 ± 0.014	1.163 ± 0.015	⋯	2.03
8088.9863	0.1929	1.071 ± 0.015	1.448 ± 0.022	0.760 ± 0.016	2.158 ± 0.014	0.437 ± 0.018	1.91
8088.9991	0.1961	1.112 ± 0.017	1.496 ± 0.019	0.764 ± 0.018	2.363 ± 0.012	0.479 ± 0.011	1.96
8089.0119	0.1993	1.125 ± 0.019	1.513 ± 0.017	0.772 ± 0.012	2.310 ± 0.009	0.392 ± 0.020	1.96
8089.0246	0.2025	1.115 ± 0.017	1.481 ± 0.021	0.784 ± 0.016	2.307 ± 0.012	0.456 ± 0.016	1.90
8089.0374	0.2058	1.104 ± 0.014	1.466 ± 0.018	0.770 ± 0.014	2.355 ± 0.011	0.457 ± 0.018	1.90
8089.0502	0.2090	1.140 ± 0.015	1.481 ± 0.022	0.746 ± 0.021	2.316 ± 0.016	0.463 ± 0.015	1.99
8089.0630	0.2122	1.137 ± 0.019	1.466 ± 0.020	0.739 ± 0.018	2.255 ± 0.012	0.468 ± 0.017	1.98
8089.0757	0.2154	1.116 ± 0.020	1.452 ± 0.019	0.728 ± 0.015	2.310 ± 0.018	0.467 ± 0.013	1.99
8089.0885	0.2186	1.151 ± 0.016	1.442 ± 0.021	0.738 ± 0.013	2.352 ± 0.014	0.471 ± 0.019	1.95
8089.1013	0.2219	1.138 ± 0.019	1.474 ± 0.017	0.780 ± 0.020	2.157 ± 0.012	0.469 ± 0.016	1.90
8089.1140	0.2251	1.187 ± 0.018	1.484 ± 0.018	0.755 ± 0.019	2.149 ± 0.011	0.465 ± 0.016	1.97
8092.9513	0.1927	1.046 ± 0.016	1.303 ± 0.019	0.702 ± 0.022	1.994 ± 0.009	0.287 ± 0.018	1.86
8092.9641	0.1959	1.015 ± 0.022	1.320 ± 0.020	0.709 ± 0.017	1.994 ± 0.014	0.265 ± 0.014	1.86
8092.9769	0.1992	0.975 ± 0.016	1.292 ± 0.023	0.705 ± 0.019	1.983 ± 0.017	0.273 ± 0.020	1.83
8092.9896	0.2024	0.975 ± 0.020	1.320 ± 0.019	0.698 ± 0.016	1.903 ± 0.011	0.271 ± 0.016	1.89
8093.0024	0.2056	0.965 ± 0.022	1.353 ± 0.020	0.706 ± 0.018	1.911 ± 0.013	0.276 ± 0.019	1.92
8093.0152	0.2088	0.953 ± 0.016	1.348 ± 0.018	0.693 ± 0.012	1.791 ± 0.021	0.268 ± 0.015	1.95
8093.0280	0.2120	0.963 ± 0.019	1.300 ± 0.024	0.676 ± 0.017	1.870 ± 0.012	0.265 ± 0.018	1.92
8093.0407	0.2153	0.957 ± 0.021	1.311 ± 0.023	0.674 ± 0.014	1.873 ± 0.011	0.267 ± 0.017	1.95
8093.0536	0.2185	0.957 ± 0.019	1.305 ± 0.019	0.708 ± 0.019	1.842 ± 0.012	0.264 ± 0.013	1.84
8093.0665	0.2218	0.954 ± 0.017	1.271 ± 0.022	0.693 ± 0.023	1.986 ± 0.021	0.266 ± 0.013	1.83
8093.0793	0.2250	0.982 ± 0.018	1.280 ± 0.020	0.674 ± 0.021	1.958 ± 0.011	0.258 ± 0.017	1.90
8093.0927	0.2284	0.963 ± 0.014	1.294 ± 0.018	0.683 ± 0.018	1.912 ± 0.013	0.260 ± 0.015	1.89
8093.1056	0.2316	0.973 ± 0.019	1.345 ± 0.024	0.675 ± 0.016	1.982 ± 0.011	0.257 ± 0.018	1.99
8093.1183	0.2348	0.982 ± 0.017	1.322 ± 0.019	0.688 ± 0.015	2.003 ± 0.014	0.258 ± 0.016	1.92
8093.9399	0.4420	0.895 ± 0.020	1.117 ± 0.022	0.696 ± 0.019	0.912 ± 0.011	⋯	1.60
8093.9526	0.4452	0.898 ± 0.018	1.136 ± 0.020	0.674 ± 0.010	0.919 ± 0.011	⋯	1.69
8093.9655	0.4484	0.894 ± 0.016	1.156 ± 0.022	0.678 ± 0.014	0.859 ± 0.012	⋯	1.71
8093.9782	0.4517	0.892 ± 0.013	1.164 ± 0.019	0.662 ± 0.012	0.870 ± 0.015	⋯	1.76
8094.9617	0.6997	0.897 ± 0.019	1.067 ± 0.020	0.644 ± 0.016	1.484 ± 0.012	0.215 ± 0.016	1.66
8094.9873	0.7061	0.928 ± 0.015	1.074 ± 0.022	0.633 ± 0.021	1.441 ± 0.017	0.214 ± 0.015	1.70
8095.0129	0.7126	0.914 ± 0.021	1.087 ± 0.018	0.641 ± 0.019	1.542 ± 0.015	0.251 ± 0.019	1.70
8095.0384	0.7190	0.940 ± 0.017	1.134 ± 0.021	0.633 ± 0.013	1.621 ± 0.033	0.248 ± 0.012	1.79
8095.0652	0.7258	0.908 ± 0.026	1.136 ± 0.025	0.608 ± 0.021	1.677 ± 0.041	0.183 ± 0.017	1.87
8095.0907	0.7322	0.898 ± 0.029	1.141 ± 0.027	0.612 ± 0.019	1.560 ± 0.009	0.153 ± 0.014	1.86
8095.1163	0.7386	0.871 ± 0.018	1.165 ± 0.035	0.574 ± 0.014	1.351 ± 0.012	0.150 ± 0.021	2.03

Table 2
(Continued)

HJD (2,450,000+)	Phase	EW(Å)					$\frac{EW(\lambda8542)}{EW(\lambda8498)}$
		Ca II λ8662	Ca II λ8542	Ca II λ8498	H_α	H_β	
8095.9481	0.9484	0.827 ± 0.020	1.147 ± 0.018	0.618 ± 0.012	1.246 ± 0.017	···	1.86
8096.9554	0.2024	1.046 ± 0.017	1.401 ± 0.020	0.747 ± 0.011	1.551 ± 0.018	0.251 ± 0.018	1.88
8096.9886	0.2108	1.074 ± 0.019	1.516 ± 0.019	0.773 ± 0.018	1.501 ± 0.012	···	1.96
8097.0217	0.2191	1.071 ± 0.016	1.417 ± 0.023	0.717 ± 0.012	1.667 ± 0.027	0.261 ± 0.020	1.98
8097.0825	0.2345	1.083 ± 0.021	1.457 ± 0.021	0.755 ± 0.015	1.560 ± 0.011	···	1.93
8097.1081	0.2409	1.104 ± 0.018	1.459 ± 0.017	0.738 ± 0.019	1.783 ± 0.013	···	1.98
8098.9470	0.7046	1.087 ± 0.022	1.379 ± 0.020	0.743 ± 0.016	2.200 ± 0.009	0.360 ± 0.013	1.86
8098.9726	0.7111	1.077 ± 0.021	1.324 ± 0.018	0.728 ± 0.013	2.174 ± 0.014	0.348 ± 0.018	1.82
8098.9982	0.7175	1.111 ± 0.023	1.374 ± 0.021	0.743 ± 0.021	2.294 ± 0.017	0.368 ± 0.015	1.85
8099.0238	0.7240	1.144 ± 0.018	1.377 ± 0.017	0.745 ± 0.017	2.190 ± 0.012	0.378 ± 0.019	1.85
8099.0494	0.7304	1.142 ± 0.019	1.399 ± 0.020	0.773 ± 0.018	2.286 ± 0.011	0.388 ± 0.020	1.81
8099.0749	0.7369	1.112 ± 0.017	1.432 ± 0.019	0.758 ± 0.011	2.147 ± 0.015	0.344 ± 0.017	1.90
			2018 Nov				
8444.0112	0.7176	0.866 ± 0.026	0.986 ± 0.028	0.649 ± 0.016	1.146 ± 0.019	0.141 ± 0.019	1.52
8444.0376	0.7242	0.865 ± 0.016	1.011 ± 0.038	0.637 ± 0.013	1.190 ± 0.013	0.172 ± 0.013	1.59
8444.0704	0.7325	0.893 ± 0.025	1.033 ± 0.037	0.652 ± 0.015	1.162 ± 0.019	0.237 ± 0.016	1.58
8444.0956	0.7389	0.874 ± 0.012	1.008 ± 0.033	0.655 ± 0.017	1.214 ± 0.015	0.191 ± 0.018	1.54
8444.1191	0.7448	0.856 ± 0.009	1.008 ± 0.032	0.638 ± 0.014	1.232 ± 0.015	0.188 ± 0.015	1.58
8444.1427	0.7508	0.873 ± 0.014	1.017 ± 0.032	0.647 ± 0.016	1.154 ± 0.013	0.179 ± 0.017	1.57
8445.9850	0.2153	0.950 ± 0.023	1.168 ± 0.011	0.730 ± 0.013	1.716 ± 0.023	0.255 ± 0.011	1.60
8446.0089	0.2213	0.940 ± 0.011	1.180 ± 0.018	0.724 ± 0.015	1.831 ± 0.024	0.283 ± 0.019	1.63
8446.0327	0.2274	0.936 ± 0.015	1.165 ± 0.022	0.711 ± 0.012	1.721 ± 0.019	0.295 ± 0.013	1.64
8446.0565	0.2333	0.928 ± 0.011	1.156 ± 0.013	0.691 ± 0.016	1.600 ± 0.020	0.295 ± 0.020	1.67
8446.0825	0.2399	0.932 ± 0.011	1.159 ± 0.015	0.705 ± 0.014	1.314 ± 0.019	0.225 ± 0.016	1.64
8446.1065	0.2460	0.933 ± 0.012	1.141 ± 0.014	0.721 ± 0.017	1.302 ± 0.022	0.214±0.013	1.58
8446.1305	0.2520	0.923 ± 0.012	1.145 ± 0.009	0.704 ± 0.019	1.281 ± 0.018	0.225 ± 0.019	1.63
8446.1540	0.2579	0.911 ± 0.013	1.141 ± 0.010	0.699 ± 0.016	1.207 ± 0.023	0.234 ± 0.022	1.63
8447.9733	0.7167	0.848 ± 0.011	0.964 ± 0.022	0.728 ± 0.018	0.879 ± 0.017	0.072 ± 0.017	1.32
8447.9973	0.7227	0.872 ± 0.008	1.008 ± 0.039	0.676 ± 0.033	0.920 ± 0.015	0.083 ± 0.015	1.49
8448.0208	0.7287	0.849 ± 0.012	1.016 ± 0.037	0.722 ± 0.019	0.895 ± 0.019	0.079 ± 0.014	1.41
8448.0443	0.7346	0.873 ± 0.017	1.035 ± 0.036	0.714 ± 0.020	0.945 ± 0.012	0.105 ± 0.020	1.45
8448.0678	0.7405	0.855 ± 0.011	1.036 ± 0.037	0.708 ± 0.028	0.976 ± 0.015	0.130 ± 0.018	1.46
8448.0914	0.7465	0.860 ± 0.010	1.033 ± 0.025	0.726 ± 0.022	0.959 ± 0.010	0.126 ± 0.019	1.42
8448.1161	0.7527	0.889 ± 0.018	1.052 ± 0.034	0.753 ± 0.032	1.116 ± 0.011	0.143 ± 0.017	1.40
			2018 Aug, TIGRE				
8352.7357	0.7011	1.016 ± 0.019	1.299 ± 0.020	0.824 ± 0.022	1.216 ± 0.019	0.245 ± 0.013	1.58
8354.8769	0.2411	1.022 ± 0.022	1.287 ± 0.019	0.812 ± 0.020	1.644 ± 0.021	0.289 ± 0.018	1.58
8358.7448	0.2164	1.103 ± 0.017	1.573 ± 0.023	0.866 ± 0.027	1.202 ± 0.018	0.253 ± 0.015	1.82
			2018 Nov, TIGRE				
8446.5443	0.3564	0.989 ± 0.022	1.371 ± 0.013	0.860 ± 0.021	1.800 ± 0.017	0.323 ± 0.017	1.59
8447.5445	0.6086	0.888 ± 0.027	1.228 ± 0.020	0.758 ± 0.019	0.745 ± 0.022	0.215 ± 0.021	1.62
8449.5440	0.1128	1.022 ± 0.021	1.328 ± 0.025	0.839 ± 0.015	1.157 ± 0.019	0.236 ± 0.019	1.58

(This table is available in its entirety in machine-readable form.)

Furthermore, Zhang & Gu (2008) simultaneously analyzed several chromospheric activity indicators, including Ca II IRT, H_α, Na I D_1, D_2 doublet, and He I D_3 lines, and found that the chromospheric activity emissions of the Ca II λ8542, λ8662, and H_α lines are stronger near the two quadratures of the SZ Psc system.

Because the K1 IV primary is very active in the SZ Psc system, we assumed that the chromospheric activity variation is mainly associated with this star. Variability of chromospheric emission with the orbital phase indicates that the distribution of active regions does not uniformly appear over the stellar surface, which can help us to derive the location of active regions. During our long-term observations, there are some observing runs which have better phase coverage, and therefore we can analyze the possible rotational modulation of chromospheric activity. We group the observations of each observing run together and then plot the EWs of H_α and Ca II IRT subtraction spectra as a function of orbital phase for each observing run in Figure 5. For 2015 October–November, the observing run covers two orbital cycles that have a similar variable trend in the chromospheric activity variation. The chromospheric activity level is stronger in the first half of the orbital phase and in the second cycle. For the 2016 November observing run, it can be seen that the observations reveal stronger chromospheric emission in the first half of the orbital phase, similar with the 2015 observations, and there seems to

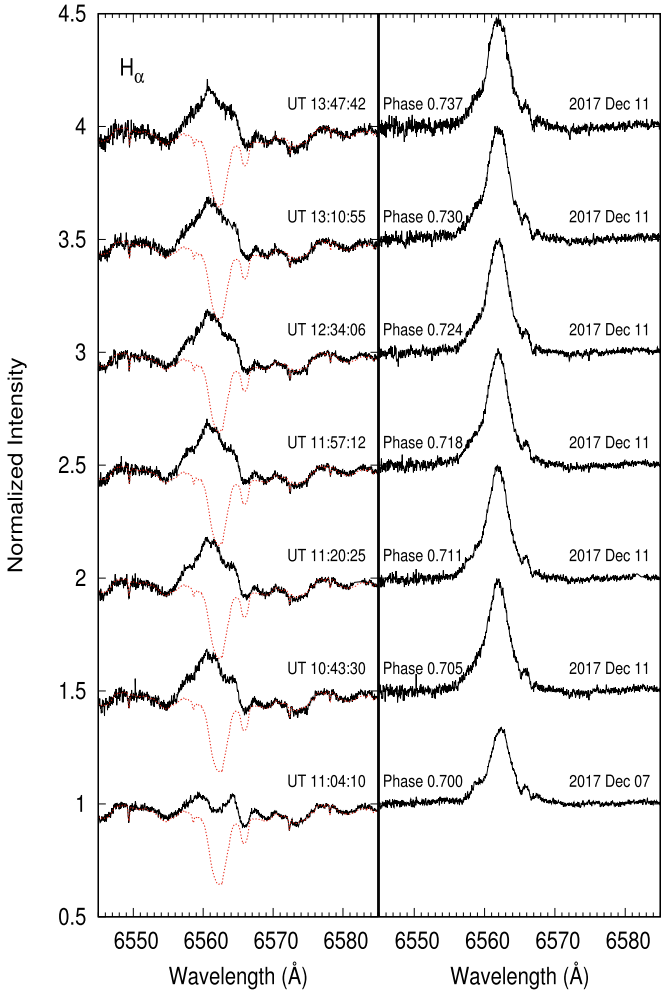

Figure 4. H_α line profiles obtained during the flare and in a quiescent state (the bottom one). The observed spectra (solid lines) and the synthesized ones (dotted lines) are plotted in the left panel and the subtracted spectra in the right one. The observing time (UT), the orbital phase, and the observing date are also marked in the plot.

be an active longitude located near phase 0.4. However, in 2016 December, the chromospheric activity variation is very different from the November observing run and there seems to be two active longitudes around the two quadratures of the SZ Psc system. For the 2017 November–December observing run at the Xinglong 2.16 m telescope, we have long-term observations that covered four orbital cycles. Although the chromospheric activity level is much more different among the different cycles, there are two active longitudes around the two quadratures of the SZ Psc system and an optical flare happened near the second quadrature. Moreover, for the 2017 November observing run at the Lijiang 2.4 m telescope, similar chromospheric activity variation was presented as in the Xinglong observations. For the 2018 November observing run, it can be seen the level of chromospheric activity is higher near phase 0.25 than near phase 0.75.

For most of the time, there are usually two chromospheric activity longitudes around the two quadratures of the SZ Psc system during our observations, consistent with the findings of Zhang & Gu (2008). Moreover, the results of the 2015 October–November and 2017 November–December observing runs show that there are significant changes in the chromospheric activity level during a few orbital cycles, similar with the finding derived by Eaton & Henry (2007).

In Figure 6, showing EWs of the H_α subtraction against the HJD for HiRES observations, it can be seen that the chromospheric activity level in 2014 is much lower than the other observing runs, which means that there seems to be a long-term variation of chromospheric activity. For the SZ Psc system, a longer-term activity cycle with a period of about 30 yr was found by Lanza et al. (2001) based on a sequence of photometric *V*-band light curves from 1957 to 1998. Therefore, to infer its possible chromospheric activity cycle, we may need frequent observations over many years in the future.

4. Excess Absorption Features

4.1. Presence of the Excess Absorption Features

The SZ Psc system often shows an extremely variable and complicated H_α line profile, and the special interesting point is that there are some unusual excess absorption features presented in the subtracted spectra at some orbital phases during our observations. We plot a time series of the observed and subtracted H_α line profiles in Figure 7 and correct the subtracted spectra to the rest velocity frame of the K1 IV primary star of the SZ Psc system, where the excess absorption features are indicated by the arrows.

Especially around the phases from 0.7799 to 0.8420 observed on 2015 October 30, where the two components of the system are separated, there is a noticeable excess absorption feature appearing in the red wing of the subtracted H_α line spectra located near the position of the F8 V secondary star of the SZ Psc system. Moreover, at the same time, a much stronger and faster evolved absorption feature appears around the He I D_3 line region in both observed and subtracted spectra, displayed in Figure 8, which is also associated with the F8 V star. For the excess absorption features, it could be found that the velocity of the excess absorption features showed gradually blueward motion relative to the K1 IV primary star and the intensity of the excess absorption decreased with time during the process. In addition to appearing like an absorption feature cospatial with plages in the Sun (Landman 1981), the He I D_3 line is also seen in the absorption features of surges and eruptive prominences (Zirin 1988). Therefore, the H_α excess absorption and strong He I D_3 line absorption could be from the absorbing material such as prominence around the SZ Psc system to some extent, when the material is seen in projection against the stellar disk. Furthermore, such similar unusual excess absorption features could also be found in the subtracted spectra of the Ca II IRT and H_β lines.

Besides the absorption feature presented on October 30, moreover, there are also some other excess absorption features superimposed on the subtracted H_α emission line profile on 2015 October 29 and November 2 (as indicated by the arrows in Figure 7), which are at phases between 0.55 and 0.60 where two components of the SZ Psc system are just separated and the primary star is in the back. Moreover, it could be found that the radial velocity of the excess absorption features showed gradually redward motion relative to the K1 IV primary star during the process.

Furthermore, for some of our observations on 2015 November 1 around orbital phase 0.3, an excess absorption feature appeared on the blue edge of the subtracted H_α profile

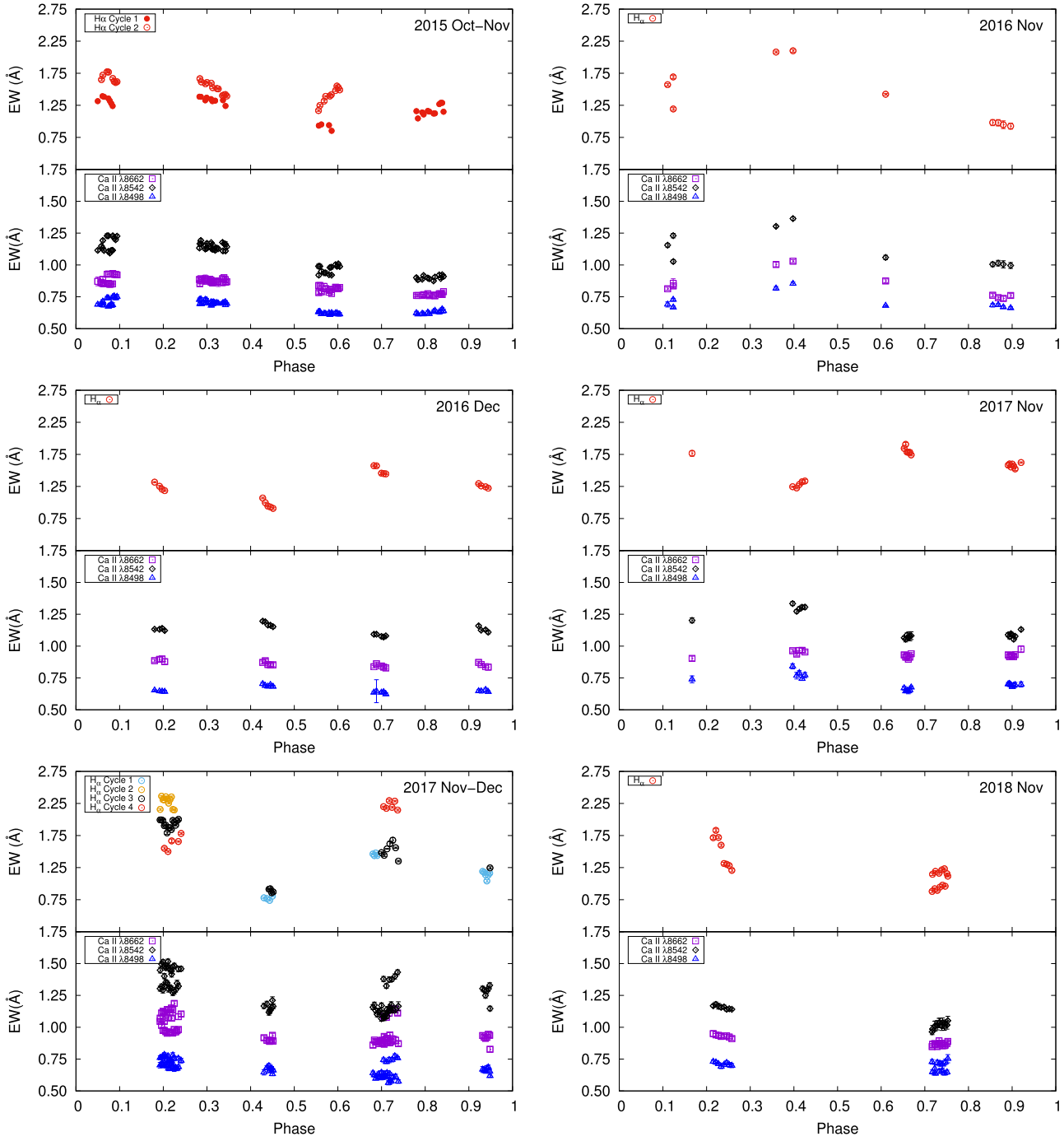

Figure 5. EWs of the subtraction profiles vs. orbital phase for the H_α and Ca II IRT lines. The labels identifying each chromospheric activity indicator are marked in the corresponding plot.

and even below the continuum level; an example is shown in Figure 9.

The radial velocities of the excess absorption features relative to the K1 IV primary star of the SZ Psc system in the chromospheric activity indicators H_α and He I D_3 lines are measured and then plotted against the orbital phase in Figure 10. However, for the excess absorption on November 1, it is difficult to measure its' radial velocity. As shown in Figure 9, we assume that the excess absorption feature may result from non-chromospheric activity superimposed on the emission profile, and therefore use one absorption Gaussian profile representing the excess absorption and several emission ones modeling the chromospheric activity emission to fit the subtracted H_α profile. And then, the radial velocities of the excess absorption relative to the K1 IV primary star are measured. For the fitted profiles, the main emission profiles presumably rise from the active chromosphere of the primary and secondary star of the SZ Psc system and the other emission profiles are probably caused by very local activity regions over the surface of the system similar to the plage-like regions in the solar case. Moreover, we also plot the radial velocities of the F8 V secondary star relative to the K1 IV primary star of SZ Psc derived by our 2015 and 2016 observations in Figure 10.

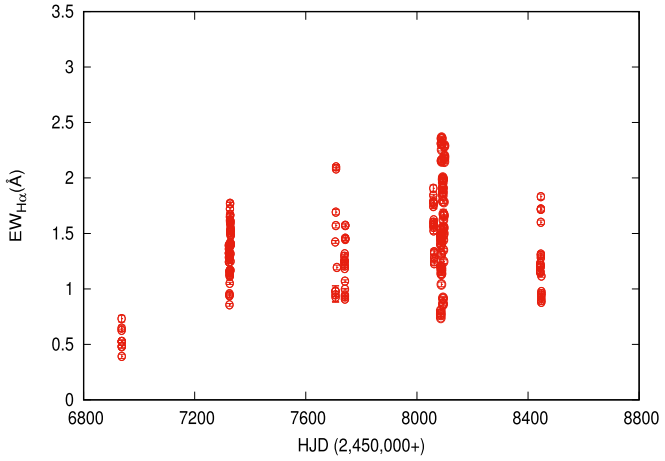

Figure 6. EWs of the H_α subtraction profiles vs. HJD of our observations.

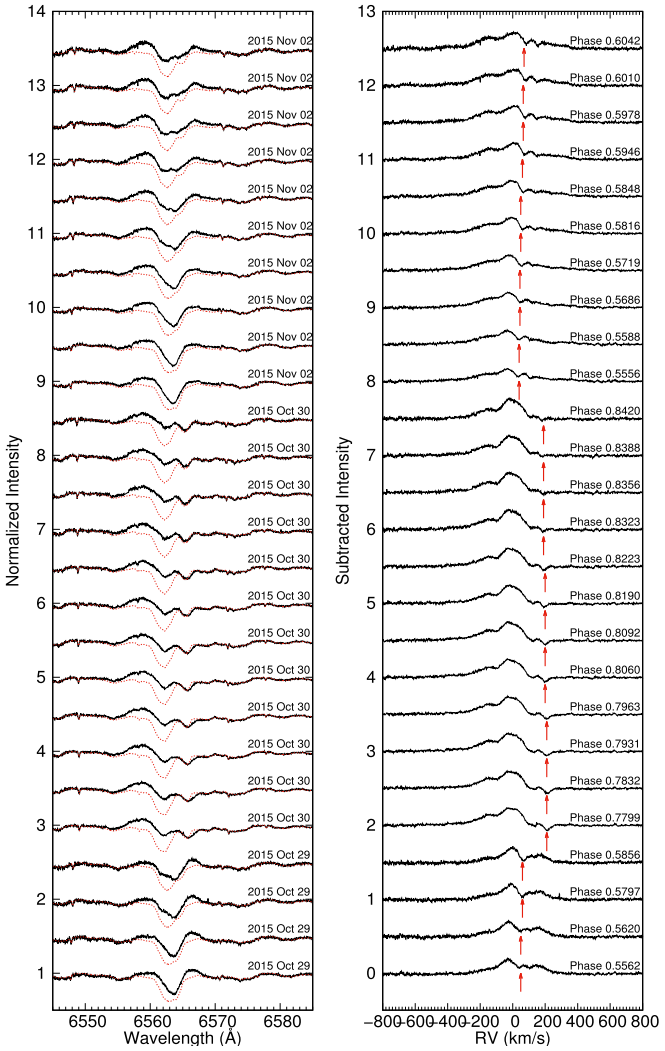

Figure 7. Time-series spectra of the H_α line. The subtracted spectra are corrected to the rest velocity frame of the K1 IV primary star of the SZ Psc system. Spectra are shifted arbitrarily for better visibility. The arrows indicate the absorption feature and the phases are also marked in the plot.

4.2. Origin of the Excess Absorption Features

For the SZ Psc system, excess absorption features in the subtracted H_α line profiles caused by prominence material had been discussed by Zhang & Gu (2008) and Cao & Gu (2012). In C19, moreover, we detected an excess absorption feature presented in the series of the subtracted H_α line spectra and interpreted it as a result of active prominence that is rising its height along the line of our sight, which is possibly associated with an strong optical flare eruption. Therefore, these mean that prominence activity may be a common feature on the SZ Psc system.

Because the K1 IV primary star is very active in the SZ Psc system, we infer that there is a prominence that is associated with this star and therefore resulted in the excess absorption features which can be detected in projection against a significant fraction of the stellar disk. For the excess absorption

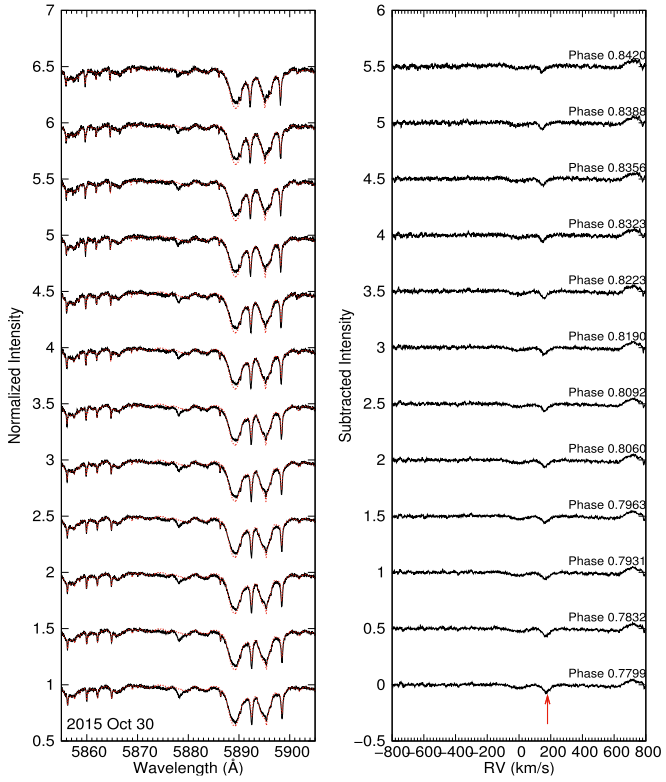

Figure 8. Same as Figure 7, but for the He I D_3 line obtained on 2015 October 30.

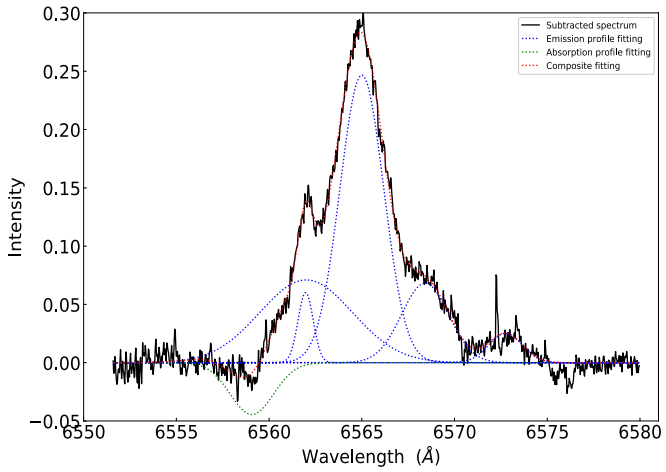

Figure 9. Example of fitting the subtracted H_α line profile using Gaussian profiles, where the solid line is the subtracted spectra and the dotted lines represent the fitted profiles.

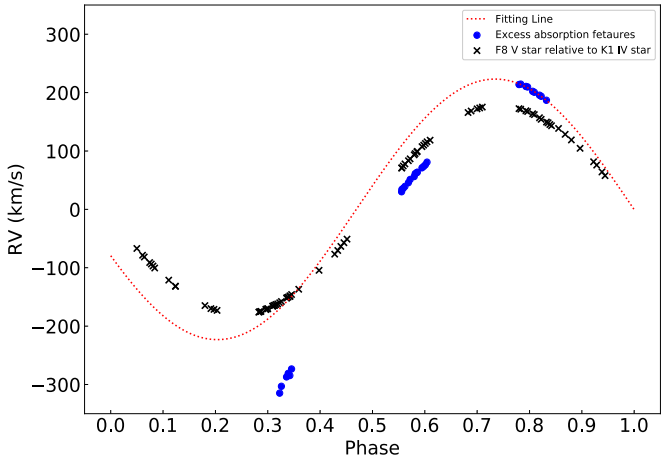

Figure 10. Radial velocities of excess absorption relative to the K1 IV primary star of the SZ Psc system.

feature presented in October 30, we can interpret it as caused by prominence material that is absorbing the chromospheric emission and continuum from the F8 V secondary star, because the absorption feature appears near the velocity of the secondary star and the blueward motion of the excess absorption feature is similar to the F8 V star relative to the K1 IV primary star. Due to the prominence material that could be projected against the disk of the secondary on October 30 and since the geometry of the SZ Psc system is well established, we can try to make a limit on the physical extent of the prominence. At phase 0.7799, the separation between the limbs of the two components of the system in the plane of the sky is about 6.7 $R_\odot$ ($\simeq$1.12R_p), which means that the prominence material extends at least up to this value from the surface of the primary. For the estimation, we adopt for the primary and secondary components the values of the parameters from Eaton & Henry (2007): $R_p = 6.0\ R_\odot$, $R_s = 1.52\ R_\odot$, $i = 69°$, $a = 15.2\ R_\odot$.

However, for excess absorption features on October 29 and November 2, they were probably caused by a prominence that is associated with the K1 IV primary star and projected on its disk. Therefore, the prominence is absorbing the emission from the active chromosphere of the K1 IV primary star. There are two reasons to support this point: first, the excess absorption feature is near the velocity of the primary star, and second, the absorption feature has redward motion relative to the K1 IV primary star during the process, just like a prominence crossing the stellar disk and scattering the chromospheric emission out of the line of sight.

We have assumed a simple model that there are prominences associated and corotated with the K1 IV primary star of the SZ Psc system that can absorb the chromospheric emission and continuum from the primary star and even the secondary one. As shown in Figure 10, if the same prominence caused the excess absorption features presented on 2015 October 30 and 29 and November 2, we could use a same sine curve to fit their radial velocities well. The reality, however, is that a sine curve could not connect them, which indicates that there are two different prominences resulting in these absorption features. For the prominence resulting in excess absorption features on October 29 and November 2, according to the method and formula of Collier Cameron & Robinson (1989a), we estimated that the distance of the prominence from the surface of the primary is about 0.97 R_p. This distance could not up to the minimum value obtained for the prominence on October 30, which means that they are different ones.

Finally, for the excess absorption features that appeared on 2015 November 1 around orbital phase 0.3, it could be caused by another prominence event. Because the absorption appears near the velocity of the F8 V secondary star, we interpret it as a prominence that is associated with the K1 IV star and was absorbing the emission and continuum from the secondary star. When the prominence could project against the disk of the secondary around phase 0.3, it must extend at least up to 7.4 $R_\odot$ ($\simeq$1.23R_p) from the surface of the primary.

5. Summary

From the above analysis of our long-term high-resolution spectroscopic observations of the very active RS CVn star SZ Psc system, the following main results are obtained.

1. Our observations of SZ Psc have shown the expected excess emission feature in several chromospheric activity indicators, and the chromospheric emission is mainly associated with the K1 IV primary star of the system, consistent with previous findings reported by several authors. The F8 V secondary star also shows chromospheric emission, but it is less active.
2. Emission feature of the He I D_3 line supported the occurrence of an optical flare in 2017 December 11. The other chromospheric activity indicators also show a stronger emission feature during the flare. Moreover, we have estimated the flare energy released in the H_α line.
3. Two chromospheric activity longitudes around the two quadratures of the SZ Psc system are observed for most of the time during our observations, and it could be found that there are significant changes in chromospheric activity during a few orbital cycles in the 2015 October–November and 2017 November and December observing runs. Moreover, the chromospheric activity level seems to show a long-term variation.
4. Of special interest is some excess absorption features in the subtracted spectra, which are probably caused by prominences associated with the K1 IV primary star. The prominence can absorb the chromospheric emission and continuum from the primary and even the secondary star, and we also discussed the implied physical extent of the prominences on the SZ Psc system.

Now, it is clear that the outer layer of the SZ Psc system is quite dynamic due to the magnetic field. To understand its chromosphere and prominences, the dense data sampling through high-resolution spectroscopy is really needed in the near future, which could be realized to utilize several telescopes located in different sites.

We would like to thank all the staff of the 2.16 m telescope at the Xinglong station of National Astronomical Observatories and the 2.4 m telescope at the Lijiang station of Yunnan Observatories for their help and support during our observations. This work is partially supported by the Open Project Program of the Key Laboratory of Optical Astronomy, National Astronomical Observatories, Chinese Academy of Sciences. Funding for the 2.4 m telescope has been provided by the Chinese Academy of Sciences and the People's Government of Yunnan Province. We also thank the anonymous

referee for helpful comments and suggestions, which led to the significant improvement of our manuscript. The joint research project between Yunnan Observatories and Hamburg Observatory is funded by Sino-German Center for Research Promotion (GZ1419). The present study is also financially supported by the National Natural Science Foundation of China under grants Nos. 10373023, 10773027, 11333006, U1531121, and 11903074, the Chinese Academy of Sciences through project No. KJCX2-YW-T24, and the West Light Foundation of the Chinese Academy of Sciences.

ORCID iDs

Dongtao Cao https://orcid.org/0000-0002-3534-1740

References

Barden, S. C. 1985, ApJ, 295, 162
Barnes, J. R., Collier Cameron, A., James, D. J., & Donati, J.-F. 2000, MNRAS, 314, 162
Berdyugina, S. V., Ilyin, I., & Tuominen, I. 1999, A&A, 349, 863
Bopp, B. W. 1981, AJ, 86, 771
Byrne, P. B., Eibe, M. T., & Rolleston, W. R. J. 1996, A&A, 311, 651
Cao, D. T., & Gu, S. H. 2012, A&A, 538, 130
Cao, D. T., & Gu, S. H. 2014, AJ, 147, 38
Cao, D. T., & Gu, S. H. 2015, MNRAS, 449, 1380
Cao, D. T., & Gu, S. H. 2017, RAA, 17, 055C
Cao, D. T., Gu, S. H., Ge, J., et al. 2019, MNRAS, 482, 988
Catalano, S., & Frasca, A. 1994, A&A, 287, 575
Collier Cameron, A., & Robinson, R. D. 1989a, MNRAS, 236, 57
Collier Cameron, A., & Robinson, R. D. 1989b, MNRAS, 238, 657
Collier Cameron, A., & Woods, J. A. 1992, MNRAS, 258, 360n
Donati, J.-F., Mengel, M., Carter, B. D., et al. 2000, MNRAS, 316, 699
Dunstone, N. J., Barnes, J. R., Collier Cameron, A., & Jardine, M. 2006, MNRAS, 365, 530
Eaton, J. A., & Hall, D. S. 1979, ApJ, 227, 907
Eaton, J. A., & Henry, G. W. 2007, PASP, 119, 259
Eibe, M. T. 1998, A&A, 337, 757
Fan, Y. F., Bai, J. M., Zhang, J. J., et al. 2015, RAA, 15, 918
Fernández-Figueroa, M. J., De Castro, E., Montesinos, B., et al. 1986, AdSpR, 6, 187
Frasca, A., Biazzo, K., Taş, G., Evren, S., & Lanzafame, A. C. 2008, A&A, 479, 557
Frasca, A., & Catalano, S. 1994, A&A, 284, 883
Gálvez, M. C., Montes, D., Fernández-Figueroa, M. J., De Castro, E., & Cornide, M. 2009, AJ, 137, 3965
García-Alvarez, D., Foing, B. H., Montes, D., et al. 2003, A&A, 397, 285
Glazunova, L. V., Yushchenko, A. V., Tsymbal, V. V., et al. 2008, AJ, 136, 1736
Gu, S.-H., & Tan, H.-S. 2003, in The Future of Cool-star Astrophysics: 12th Cambridge Workshop on Cool Stars, Stellar Systems, and the Sun, ed. A. Brown, G. M. Harper, & T. R. Ayres (Boulder, CO: Univ. Colorado), 986
Gu, S. H., Tan, H. S., Shan, H. G., & Zhang, F. H. 2002, A&A, 388, 889
Hall, J. C. 1996, PASP, 108, 313
Hall, J. C., & Ramsey, L. W. 1992, AJ, 104, 1942
Huenemoerder, D. P., & Ramsey, L. W. 1984, AJ, 89, 549
Huenemoerder, D. P., & Ramsey, L. W. 1987, ApJ, 319, 392
Jakate, S. M., Bakos, G. A., Fernie, J. D., & Heard, J. F. 1976, AJ, 81, 250
Jeffries, R. D. 1993, MNRAS, 262, 369
Kang, Y. W., Lee, W.-B., Kim, H., & Oh, K.-D. 2003, MNRAS, 344, 1227
Landman, D. A. 1981, ApJ, 244, 345
Lanza, A. F., Rodonò, M., Mazzola, L., & Messina, S. 2001, A&A, 376, 1011
López-Santiago, J., Montes, D., Fernandez-Figueroa, M. J., & Ramsey, L. W. 2003, A&A, 411, 489
Messina, S. 2008, A&AS, 480, 495
Mittag, M., Hempelmann, A., González-Pérez, J. N., & Schmitt, J. H. M. M. 2010, AdAst, 2010, 6
Montes, D., Fernández-Figueroa, M. J., De Castro, E., & Cornide, M. 1995a, A&A, 294, 165
Montes, D., Fernández-Figueroa, M. J., De Castro, E., & Cornide, M. 1995b, A&AS, 109, 135
Montes, D., Fernández-Figueroa, M. J., De Castro, E., & Sanz-Forcada, J. 1997, A&AS, 125, 263
Montes, D., Fernández-Figueroa, M. J., De Castro, E., et al. 2000, A&AS, 146, 103
Montes, D., Sanz-Forcada, J., Fernández-Figueroa, M. J., & Lorente, R. 1996, A&A, 310, L29
Oláh, K. 2006, Ap&SS, 304, 145
Popper, D. M. 1988, AJ, 96, 1040
Ramsey, L. W., & Nations, H. L. 1981, PASP, 93, 732
Robinson, R. D., & Collier Cameron, A. 1986, PASAu, 6, 308
Schmitt, J. H. M. M., Schröder, K.-P., Rauw, G., et al. 2014, AN, 335, 787
Schrijver, C. J., & Zwaan, C. 2000, Solar and Stellar Magnetic Activity (Cambridge: Cambridge Univ. Press)
Tandberg-Hanssen, E. 1967, Solar Activity (Waltham, MA: Blaisdell)
Wolter, U., Robrade, J., Schmitt, J. H. M. M., & Ness, J. U. 2008, A&A, 478, L11
Xiang, Y., Gu, S. H., Collier Cameron, A., Barnes, J. R., & Zhang, L. Y. 2016, MNRAS, 456, 314
Zhang, L. Y., & Gu, S. H. 2008, A&A, 487, 709
Zhang, L. Y., Pi, Q. F., Han, X. M. L., Chang, L., & Wang, D. M. 2016, MNRAS, 459, 854
Zirin, H. 1988, Astrophysics of the Sun (Cambridge: Cambridge Univ. Press)